DISCUSSION

Keratinocytes and fibroblasts adhere to, spread on, and can grow and survive on flat and all sizes of regular, hexagonally packed porous (ε-calprolactone) films with pores ranging in size from 3 to 20 μm. Specifically, we have demonstrated that keratinocyte attachment is dependent on the size of the pores and that cell adhesion was highest on the smallest 3-μm films. The unique characteristics of the porous patterned films account for these changes in the 2 cell types studied. Each cell type displays subtle differences due to their particular adhesion and growth characteristics, as shown by their unique repertoire of cell-adhesion receptors and cell–cell interactions with porous substrates.

Substrate characteristics, temperature, the presence of cations,[32] cell activation state, and cell viability, which is modulated by cytokines, govern keratinocyte adhesion in part. Keratinocytes in our study were more discriminating than fibroblasts and adhered best on smaller-pore-sized film (3-μm-pored films), the next best adhesion pore size being 5-μm-pore film. The explanation for these effects comes after several observations. First, if this pore size is greater than the size of the initial seeded cells, they can and do enter the film pores. Because keratinocytes require direct adjacent cell–cell contact for proper levels of growth, signaling, and cell survival, cell separation caused by the larger pores is likely to detrimentally affect these processes. It has previously been shown that keratinocytes seeded onto grafts without proper cell–cell and cell–substrate contact fail to form appropriate epidermal sheets[33] and survive in culture.[28,33] Further beneficial characteristics of the small-pore films include the fact that they have a greater surface area over which cells can adhere. Finally, the smaller pore size produces a greater length of pore edge per surface area that cells can insert their plasma membrane lamelapodia and filopodial extensions into to gain leverage and increase cell adhesion. This leverage may also inhibit cell migration. Keratinocytes require cell–cell and cell–substrate contact especially for cell growth and survival. When cells, especially keratinocytes, become isolated or removed from adjacent cell–cell contact (or are trapped in pores) readily undergo cell cycle arrest or apoptotic changes,[34] as was seen with pyknotic cells in our growth experiments. Similarly, mutations in the first human genetic disease affecting focal contact-adhesion protein kindlin-1 in skin also cause premature keratinocyte cell death by apoptosis and skin thinning and erosions.[35–37]

Our data suggest that the most important keratinocyte adhesive mechanism does not involve the proper formation of the hemidesmosome junction or the assembly of any extracellular components, including laminins 5/10[29] or matrix secretion of collagens I, IV, and VII. Conversely, fibroblasts and keratinocytes that adhered to porous films assembled highly dynamic, actin-associated focal adhesion-like structures that were observed attaching to the surface of the films. Given the short time frame over which cells, particularly fibroblasts, adhered to and spread on the films and taken together with the abundance of cytoplasmic actin filaments and focal adhesion components observed within filopodia and lamelapodia, we suggest that focal adhesions form the majority of adhesive junctions on these surfaces. The identification of fibronectin and vitronectin deposits in cultures and recent findings of the importance of focal contacts and their associated proteins on the adhesion of other cell types cultured on porous membranes further supports this hypothesis.[19,38,39]

Closely related to the film adhesive characteristics is the related ability to allow cell migration. The ability of the cells to gain leverage because of the extra length of pore edge or to enter the film pores in the small-pore samples probably affected keratinocyte and fibroblast migration rates, as previously mentioned. Our findings support previous reports that fibroblast migration on collagen sponges with various size pores was significantly greater than that of keratinocytes.[40]

In addition, we demonstrated that the smallest, 3-μm pore size was most efficient at inhibiting the transmigration of both cell types (to the opposite side of the film). Cell transmigration has important future implications in the design of monolayer or bilayer polymer grafts for the treatment of skin wounds. The beneficial adhesive properties and blocking of transmigration of the smaller pores will prove to be an important factor when this film is used to support a bilayered human skin equivalent or dermal equivalent by preventing two different cells types from mixing.

Keratinocytes are more selective than fibroblasts and grow best on small pore-sized film (3-μm-pored films). The second most effective film size for keratinocyte adhesion was the 5-μm film ($3\,\mu m > 5\,\mu m > 10\,\mu m >$ flat $>> 15\,\mu m < 20\,\mu m$). Explaining these growth effects on both cell types encompasses cell substrate adhesion and ability to migrate and form cell–cell contacts that all contributed to affect *in vitro* growth rates.[41] Our data suggested that the keratinocytes were more likely to grow poorly in isolation or in small colonies without significant all-round cell–cell contact. This would have important implications for cell contact–induced growth signals.[42,43] Other reports have also indicated that keratinocytes were more likely to grow poorly in isolation without cell–cell contact similar to that seen on porous collagen sponges.[40] Fibroblasts grew equally well on flat or small-pore-sized film but on pores larger than 10 μm showed significantly slower grow rates. Direct migration of fibroblasts on the underlying substrate was relatively short term due to formation of multiple cell layers. However, fibroblast adhesion and growth-signaling mechanisms are known to involve many of the same actin-associated focal-adhesion molecules as in keratinocytes.[44–46] NIH 3T3 fibroblasts have previously been demonstrated to adhere to all sizes of porous films.[24]

The important characteristics of porous films that cause significant changes in cell adhesion, migration, and growth rates include characteristics that enable cells to extend focal-contact plasma-membrane projections to gain adhesion and leverage that allow better growth. Further work is required to

describe the properties of PCL films with smaller pores and to determine whether further beneficial effects of adhesion, growth, and increases in keratinocyte migration rates that are observed in culture are maintained in *in vivo* wound-healing models.

ACKNOWLEDGMENTS

We thank Ms. Y. Miyamura and Ms. N. Ikeda for their excellent technical assistance in cell-film preparation, Mr. H. Nakamura and Ms. K. Sakai for their electron microscopy assistance, and Ms. Y. Morita and Ms. E. Ito for their excellent technical assistance in film fabrication and help with the migration studies. This work was supported by a grant-in-aid from the Health and Labor Sciences Research Grant (research into Human Genome, Tissue Engineering) H17-Saisei-12 (to J.R.M.) and by a grant-in-aid of Scientific Research A (17209038, H.S.) from the Japanese Society for the Promotion of Science. This work was also supported by a Health and Labor Sciences Research Grant (Research into Measures Treating Intractable Diseases) from the Ministry of Health, Labor and Welfare (H16-Nanchi-05, to H.S.) and a Project for Realization of Regenerative Medicine from the Ministry of Education, Science, Sports, and Culture of Japan (to H.S.). The hybridoma monoclonal antibody supernatants were obtained from the Developmental Studies Hybridoma Bank, developed under the auspices of the National Institute of Child Health and Development and maintained by the Department of Biological Sciences, University of Iowa, Iowa City, Iowa.

REFERENCES

1. Stenzel-Rosenbaum, M.H., Davis, T.P., Fane, A.G., and Chen, V. Porous polymer films and honeycomb structures made by the self-organization of well-defined macromolecular structures created by living radical polymerization techniques. Angew Chem Int Ed Engl **40,** 3428, 2001.
2. Zein, I., Hutmacher, D.W., Tan, K.C., and Teoh, S.H. Fused deposition modeling of novel scaffold architectures for tissue engineering applications. Biomaterials **23,** 1169, 2002.
3. Chung, T.W., Yang, M.G., Liu, D.Z., Chen, W.P., Pan, C.I., and Wang, S.S. Enhancing growth human endothelial cells on arg-gly-asp (RGD) embedded poly (epsilon-caprolactone) (PCL) surface with nanometer scale of surface disturbance. J Biomed Mater Res A **72,** 213, 2005.
4. Serrano, M.C., Pagani, R., Vallet-Regi, M., Pena, J., Ramila, A., Izquierdo, I., and Portoles, M.T. *In vitro* biocompatibility assessment of poly(epsilon-caprolactone) films using l929 mouse fibroblasts. Biomaterials **25,** 5603, 2004.
5. Ng, K.W., Khor, H.L., and Hutmacher, D.W. *In vitro* characterization of natural and synthetic dermal matrices cultured with human dermal fibroblasts. Biomaterials **25,** 2807, 2004.
6. Wake, M.C., Gupta, P.K., and Mikos, A.G. Fabrication of pliable biodegradable polymer foams to engineer soft tissues. Cell Transplant **5,** 465, 1996.
7. Wake, M.C., Patrick, C.W., Jr., and Mikos, A.G. Pore morphology effects on the fibrovascular tissue growth in porous polymer substrates. Cell Transplant **3,** 339, 1994.
8. Lee, S.J., Choi, J.S., Park, K.S., Khang, G., Lee, Y.M., and Lee, H.B. Response of mg63 osteoblast-like cells onto polycarbonate membrane surfaces with different micropore sizes. Biomaterials **25,** 4699, 2004.
9. Wan, Y., Wang, Y., Liu, Z., Qu, X., Han, B., Bei, J., and Wang, S. Adhesion and proliferation of oct-1 osteoblast-like cells on micro- and nano-scale topography structured poly(l-lactide). Biomaterials **26,** 4453, 2005.
10. Berry, C.C., Campbell, G., Spadiccino, A., Robertson, M., and Curtis, A.S. The influence of microscale topography on fibroblast attachment and motility. Biomaterials **25,** 5781, 2004.
11. O'Brien, F.J., Harley, B.A., Yannas, I.V., and Gibson, L.J. The effect of pore size on cell adhesion in collagen-gag scaffolds. Biomaterials **26,** 433, 2005.
12. Lee, S.H., Kim, B.S., Kim, S.H., Choi, S.W., Jeong, S.I., Kwon, I.K., Kang, S.W., Nikolovski, J., Mooney, D.J., Han, Y.K., and Kim, Y.H. Elastic biodegradable poly(glycolide-co-caprolactone) scaffold for tissue engineering. J Biomed Mater Res **66A,** 29, 2003.
13. Jeong, S.I., Kim, S.H., Kim, Y.H., Jung, Y., Kwon, J.H., Kim, B.S., and Lee, Y.M. Manufacture of elastic biodegradable plcl scaffolds for mechano-active vascular tissue engineering. J Biomater Sci Polym Ed **15,** 645, 2004.
14. Wald, H.L., Sarakinos, G., Lyman, M.D., Mikos, A.G., Vacanti, J.P., and Langer, R. Cell seeding in porous transplantation devices. Biomaterials **14,** 270, 1993.
15. Choi, Y.S., Hong, S.R., Lee, Y.M., Song, K.W., Park, M.H., and Nam, Y.S. Studies on gelatin-containing artificial skin: II. Preparation and characterization of cross-linked gelatin-hyaluronate sponge. J Biomed Mater Res **48,** 631, 1999.
16. Tanaka, M., Takebayashi, M., Miyama, M., Nishida, J., and Shimomura, M. Design of novel biointerfaces (II). Fabrication of self-organized porous polymer film with highly uniform pores. Biomed Mater Eng **14,** 439, 2004.
17. Saito, A., Taketani, S., Arai, K., Tanaka, M., Shimomura, M., and Sawa, Y. Highly regular honeycomb-patterned biodegradable scaffold promotes topographical control of myoblast proliferation and differentiation: A novel scaffold for myocardial regenerative therapy. J Mol Cell Cardiol **39,** 1022, 2005.
18. Tsuruma, A., Tanaka, M., Fukushima, N., and Shimomura, M. Morphological changes of neurons on self-organized honeycomb patterned films. Kobunshi Ronbunshu **61,** 628, 2004.
19. Tanaka, M., Tanakaya, A., Ito, E., Sunami, H., Yamamoto, S., and Shimomura, M. Effect of pore size of self-organized honeycomb-patterned polymer films on spreading, focal adhesion, proliferation, and function of endothelial cells. J Nanosci Nanotech **7,** 763, 2007.
20. Schwope, A.D., Wise, D.L., Sell, K.W., Dressler, D.P., and Skornick, W.A. Evaluation of wound-covering materials. J Biomed Mater Res **11,** 489, 1977.
21. Shimomura, M., Tanaka, M., Tsuruma, A., Sunami, H., and Yamamoto, S. Biomedical application of patterned polymer films prepared by self-organization. J Surf Sci Soc Jap **27,** 170, 2006.
22. Tsuruma, A., Tanaka, M., Fukushima, N., Yamamoto, S., and Shimomura, M. Morphological changes in neurons by self-organized patterned films. e-J Surf Sci Nanotech **3,** 159, 2005.

23. Tsuruma, A., Tanaka, M., Yamamoto, S., Fukushima, N., and Shimomura, M. Topographical control of neurites extension on stripe-patterned polymer films. Colloids Surf A Physicochem.Eng Asp **284–285,** 548, 2006.
24. Fukuhira, Y., Kitazono, E., Hayashi, T., Kaneko, H., Tanaka, M., Shimomura, M., and Sumi, Y. Biodegradable honeycomb-patterned film composed of poly(lactic acid) and dioleoylphosphatidylethanolamine. Biomaterials **27,** 1797, 2006.
25. Yabu, H., Takebayashi, M., Tanaka, M., and Shimomura, M. Superhydrophobic and lipophobic properties of self-organized honeycomb and pincushion structures. Langmuir **21,** 3235, 2005.
26. Tanaka, Y., Sung, K.C., Tsutsumi, A., Ohba, S., Ueda, K., and Morrison, W.A. Tissue engineering skin flaps: which vascular carrier, arteriovenous shunt loop or arteriovenous bundle, has more potential for angiogenesis and tissue generation? Plast Reconstr Surg **112,** 1636, 2003.
27. Yabu, H., Tanaka, M., Ijiro, K., and Shimomura, M. Preparation of honeycomb-patterned polyimide films by self-organization. Langmuir **19,** 6297, 2003.
28. Butler, C.E., Orgill, D.P., Yannas, I.V., and Compton, C.C. Effect of keratinocyte seeding of collagen-glycosaminoglycan membranes on the regeneration of skin in a porcine model. Plast Reconstr Surg **101,** 1572, 1998.
29. McMillan, J.R., Akiyama, M., Nakamura, H., and Shimizu, H. Colocalization of multiple laminin isoforms predominantly beneath hemidesmosomes in the upper lamina densa of the epidermal basement membrane. J Histochem Cytochem **54,** 109, 2006.
30. Richardson, K.C., Jarret, L., and Finke, E.H. Embedding in epoxy resins for ultrathin sectioning in electron microscopy. Stain Technol **35,** 313, 1960.
31. Chometon, G., Zhang, Z.G., Rubinstein, E., Boucheix, C., Mauch, C., and Aumailley, M. Dissociation of the complex between cd151 and laminin-binding integrins permits migration of epithelial cells. Exp Cell Res 2006.
32. Patel, H., Marcelo, C., Voorhees, J.J., and Diaz, L.A. *In vitro* alterations of epidermal cell adhesion induced by temperature, substrate, and cations. J Invest Dermatol **76,** 474, 1981.
33. Rompre, P., Auger, F.A., Germain, L., Bouvard, V., Lopez Valle, C.A., Thibault, J., and Le Duy, A. Influence of initial collagen and cellular concentrations on the final surface area of dermal and skin equivalents: A Box-Behnken analysis. *In Vitro* Cell Dev Biol **26,** 983, 1990.
34. Presland, R.B., Kuechle, M.K., Lewis, S.P., Fleckman, P., and Dale, B.A. Regulated expression of human filaggrin in keratinocytes results in cytoskeletal disruption, loss of cell-cell adhesion, and cell cycle arrest. Exp Cell Res **270,** 199, 2001.
35. Lanschuetzer, C.M., Muss, W.H., Emberger, M., Pohla-Gubo, G., Klausegger, A., Bauer, J.W., and Hintner, H. Characteristic immunohistochemical and ultrastructural findings indicate that kindler's syndrome is an apoptotic skin disorder. J Cutan Pathol **30,** 553, 2003.
36. Jobard, F., Bouadjar, B., Caux, F., Hadj-Rabia, S., Has, C., Matsuda, F., Weissenbach, J., Lathrop, M., Prud'homme, J.F., and Fischer, J. Identification of mutations in a new gene encoding a FERM family protein with a pleckstrin homology domain in kindler syndrome. Hum Mol Genet **12,** 925, 2003.
37. Siegel, D.H., Ashton, G.H., Penagos, H.G., Lee, J.V., Feiler, H.S., Wilhelmsen, K.C., South, A.P., Smith, F.J., Prescott, A.R., Wessagowit, V., Oyama, N., Akiyama, M., Al Aboud, D., Al Aboud, K., Al Githami, A., Al Hawsawi, K., Al Ismaily, A., Al-Suwaid, R., Atherton, D.J., Caputo, R., Fine, J.D., Frieden, I.J., Fuchs, E., Haber, R.M., Harada, T., Kitajima, Y., Mallory, S.B., Ogawa, H., Sahin, S., Shimizu, H., Suga, Y., Tadini, G., Tsuchiya, K., Wiebe, C.B., Wojnarowska, F., Zaghloul, A.B., Hamada, T., Mallipeddi, R., Eady, R.A., McLean, W.H., McGrath, J.A., and Epstein, E.H. Loss of kindlin-1, a human homolog of the caenorhabditis elegans actin-extracellular-matrix linker protein unc-112, causes kindler syndrome. Am J Hum Genet **73,** 174, 2003.
38. Yamamoto, S., Tanaka, M., Sunami, H., Yamashita, S., Morita, Y., and Shimomura, M. Relationship between adsorbed fibronectin and cell adhesion on a honeycomb-patterned film. Surf Sci in press.
39. Yamamoto, S., Tanaka, M., Sunami, H., Yamashita, S., Morita, Y., and Shimomura, M. Relationship between adsorbed fibronectin and fak activation on a honeycomb-patterned film. J Surf Sci Soc Jap in press.
40. McKegney, M., Taggart, I., and Grant, M.H. The influence of crosslinking agents and diamines on the pore size, morphology and the biological stability of collagen sponges and their effect on cell penetration through the sponge matrix. J Mater Sci Mater Med **12,** 833, 2001.
41. Dai, N.T., Williamson, M.R., Khammo, N., Adams, E.F., and Coombes, A.G. Composite cell support membranes based on collagen and polycaprolactone for tissue engineering of skin. Biomaterials **25,** 4263, 2004.
42. Zhu, A.J. and Watt, F.M. Expression of a dominant negative cadherin mutant inhibits proliferation and stimulates terminal differentiation of human epidermal keratinocytes. J Cell Sci **109 (Pt 13),** 3013, 1996.
43. Takeichi, M., Watabe, M., Shibamoto, S., and Ito, F. Cadherin-dependent organization and disorganization of epithelial architecture. Princess Takamatsu Symp **24,** 28, 1994.
44. Akiyama, S.K., Larjava, H., and Yamada, K.M. Differences in the biosynthesis and localization of the fibronectin receptor in normal and transformed cultured human cells. Cancer Res **50,** 1601, 1990.
45. Kelly, T., Molony, L., and Burridge, K. Purification of two smooth muscle glycoproteins related to integrin. Distribution in cultured chicken embryo fibroblasts. J Biolog Chem **262,** 17189, 1987.
46. Srivastava, J., Elliott, B.E., Louvard, D., and Arpin, M. Src-dependent ezrin phosphorylation in adhesion-mediated signaling. Mol Biol Cell 2005.

Address reprint requests to:
James R. McMillan, M.Sc., Ph.D.
Department of Dermatology
Hokkaido University Graduate School of Medicine
North 15 West 7, Kitaku
Sapporo 060-8638
Japan

E-mail: jrm57@med.hokudai.ac.jp

INSTITUTE OF PHYSICS PUBLISHING NANOTECHNOLOGY
Nanotechnology 18 (2007) 084010 (5pp) doi:10.1088/0957-4484/18/8/084010

Stress relaxation of HepG2 cells measured by atomic force microscopy

T Okajima[1,4], M Tanaka[1], S Tsukiyama[2], T Kadowaki[3], S Yamamoto[2], M Shimomura[1] and H Tokumoto[1]

[1] Nanotechnology Research Center, Research Institute for Electronic Science, Hokkaido University, Japan
[2] Creative Research Initiative 'Sousei', Hokkaido University, Japan
[3] Graduate School of Information Science and Technology, Hokkaido University, Japan

E-mail: okajima@es.hokudai.ac.jp

Received 24 July 2006, in final form 19 October 2006
Published 18 January 2007
Online at stacks.iop.org/Nano/18/084010

Abstract
Stress relaxation of HepG2 cells was examined with an atomic force microscope (AFM). In the measurement, a loading force was applied to the cell by an AFM tip, and a time series of the cantilever deflection signal was measured at a fixed position of the cantilever base displacement. The relaxation of the loading force was clearly observed on the HepG2 cells, and was well fitted to a stretched exponential function known as the Kohlrausch–Williams–Watts (KWW) function, which is empirically employed to represent dispersion processes of the system. The relaxation time and the stretching exponent parameter were estimated to be ~0.5 s and 0.4–0.6, respectively. The latter indicated that the relaxation observed in HepG2 cells consisted of multiple relaxation processes. Moreover, it was found that the characteristic feature of the relaxation process was not strongly correlated with the elastic properties of the cells.

(Some figures in this article are in colour only in the electronic version)

1. Introduction

Since living cells have high anisotropy as a consequence of their complex internal architecture, it is crucial to explore the relationship between structure and function at the microscale and nanoscale under physiological conditions. The atomic force microscope (AFM) is one of the instruments available not only to image the topography of living cells, but also to measure the mechanical properties and biological functions in response to mechanical stimuli [1, 2]. Elastic properties, i.e., reversible deformation of living cells, can be investigated by measuring force–distance curves, which represent the relation between the loading force and the depth of indentation as the AFM tip is pushed against the cell surface [3–9]. The Young's modulus has been quantified using the Hertz model [1] on several types of animal cell, and the spatial heterogeneity of the Young's modulus has been clearly resolved [7–9].

The viscoelastic properties, which include both the elastic and viscous effects (rheological behaviour) of cell surfaces, can be measured with the force modulation mode [10–14], which is the basis of measurement of the dynamic response of the loading force with respect to an external periodic strain. Recently, by using the force modulation mode, the complex shear modulus has been investigated in detail at 0.1–100 Hz in human lung epithelial cells [13] and airway smooth muscle cells [14].

On the other hand, it is known [5–7] that, in the force–distance curve measurement on living cells, hysteresis often appears between the approaching and retracting parts, which is mainly attributed to the dissipation of energy (viscous effects) to the cells [7]. This suggests that the viscoelastic properties of living cells can also be clarified by measuring the dc component of the cantilever deflection signal, without any external vibration.

Wu *et al* [15] have demonstrated the creep measurement of cells with AFM. In this measurement, the loading force is maintained at a constant value by controlling the cantilever base displacement, while the displacement is measured as a function of time. They have studied in detail the relationship

[4] Address for correspondence: Kitaku N21 W10, Sapporo 001-0021, Japan.

between the viscoelastic properties and the cytoskeletal architecture of L929 cells. Recently, Darling *et al* [16] have measured with AFM the stress relaxation of cells such as zonal articular chondrocytes. In this measurement, the cantilever base displacement is kept constant, while the loading force is measured as a function of time. In spite of these studies, we know little of how the magnitude of the loading force influences the relaxation process, as well as how the relaxation process correlates with the elastic properties of the cells, both of which are crucial for the application of these relaxation tests with AFM to living cells. In this study, we investigated these relationships at a local region of the cell surface by measuring the relaxation of the loading force of cells such as the human hepatoma cell line HepG2 [17].

2. Experimental details

2.1. Cell culture

HepG2 cells were cultured on a 35 mm dish in minimum essential medium (MEM) (Sigma, St Louis, MO, USA) supplemented with 2 mM glutamine, 0.06% (w/v) penicillin, 0.1% (w/v) streptomycin (GIBCO-BRL Life Technologies, Grand Island, NY, USA) and 10% (v/v) fetal bovine serum (FBS; Atlanta Biologicals, Atlanta, GA, USA) and incubated at 37 °C in a humidified 5% CO_2-containing atmosphere. After incubation on the culture dish for 2 days, the HepG2 cell samples were used for the AFM experiments.

2.2. AFM

We used a commercial AFM apparatus, MFP-3D AFM (Asylum Research, Santa Barbara, CA, USA), which was mounted on an inverted optical microscope (IX-71; Olympus Co., Japan). A silicon cantilever with a rectangular shape (38 μm long, 16 μm wide and 0.2 μm thick), 'BioLever mini' (BL-AC40TS; Olympus Co.) [18], was used. Since this cantilever was small compared with the conventional V-shaped one for measuring biological samples, the hydrodynamic drag force of this cantilever in liquid environments was greatly reduced [19]. Additionally, since the tip of this cantilever was ~7 μm in length [18], which was longer than the V-shaped cantilever, the squeezing force [20] caused by the liquids sandwiched between the cantilever and the sample surface was also reduced [19].

The spring constant of the cantilevers was determined using the thermal fluctuation method [21] as ~0.1 N m^{-1}. The resonant frequency was ~30 kHz in the culture medium. The tapping mode imaging was carried out at around the resonant frequency with a few tens of nanometres of the cantilever amplitude.

The deflection sensitivity of the optical lever was calibrated by measuring the slope of the contact region of a force–distance curve acquired on a cleaved mica surface in culture medium. The loading force was determined by multiplying the cantilever spring constant by its deflection, via Hooke's law. These calibrations were conducted prior to the cell experiments.

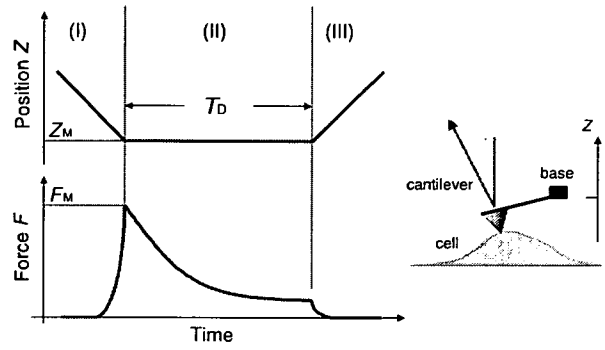

Figure 1. Schematics of the stress relaxation measurement with AFM. In region I, the AFM tip was indented into the cell surface until the loading force attained a preset trigger force F_M. In region II, the position of the cantilever base Z was kept at a constant value Z_M, and a time series of loading force data was sampled for the duration time T_D. The force curve in region III was also measured at the same scan rate as the approaching one.

2.3. Measurement of elastic properties and stress relaxation

Experiments were performed at room temperature within a few hours after placing HepG2 cell samples on the AFM sample stage. The optical microscope was used to choose a particular cell to be probed by the AFM cantilever.

Figure 1 shows a schematic picture of stress relaxation measurement with AFM. The AFM tip approached the cell surface at a scan rate of 3 μm s^{-1} until the loading force attained a trigger force, F_M, and the cantilever base displacement was fixed at Z_M for a duration time of T_D, usually 1.5 s. Then, the cantilever deflection signal was sampled with a 14-bit data acquisition board, and stored in a personal computer. The AFM tip was retracted with the same scan rate as the approaching process. The F_M was changed from 0.6 to 1.2 nN to investigate the dependence of the cell mechanical response on the loading force. These values of F_M were smaller than those of the previous creep experiment with a sharp tip [15].

In order to investigate how the relaxation process of the loading force correlates with the elastic properties of the cells, we conducted stress relaxation measurements at different positions on the cell surface. The apparent Young's modulus E of the cell and the position of the contact point between the tip and the cell surface were estimated by fitting the force curves, obtained in the approaching process, to a modified Hertz model for the elastic indentation between a stiff cone and a flat surface [23], expressed by

$$F = \frac{2}{\pi}\frac{E\tan\alpha}{(1-\nu^2)}\delta^2, \qquad (1)$$

where ν is the Poisson's ratio of the cell, δ is the indentation depth of the tip, and α is the half-opening angle of the tip apex. The α and ν were assumed to be 17.5° [18] and 0.5, respectively. The estimated position of the contact point allowed us to know the height of the cell at the measurement position. In order to minimize the effect of the solid substrate [22], the experimental data measured on a central region of a cell were analyzed and shown below.

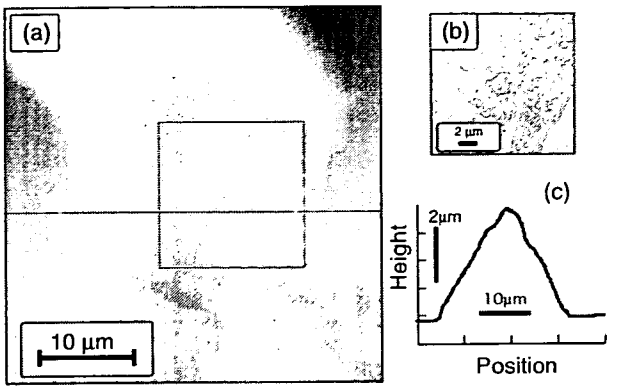

Figure 2. (a) Tapping mode topographic image of HepG2 cells cultured on collagen-coated dishes. Scan size was 40 × 40 μm. (b) Amplitude error image of a particular part of the cell indicated by the rectangle in (a). (c) Line profile of the cell topography indicated by the line in (a).

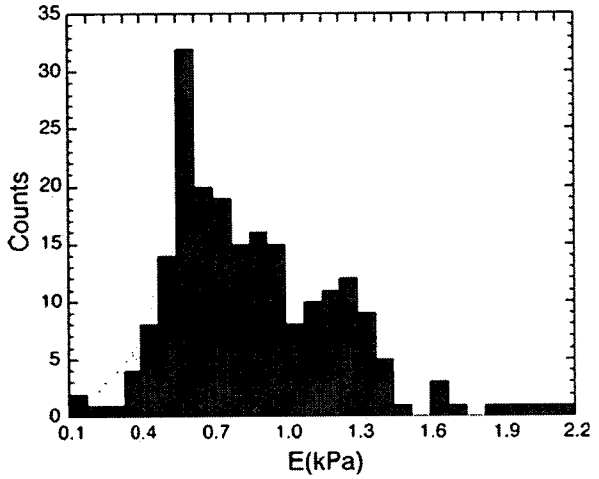

Figure 3. Histogram of Young's modulus E of HepG2 cells shown in figure 2, estimated by force–distance curve measurements.

3. Results and discussion

Figure 2(a) shows the tapping mode topographic image of HepG2 cells in culture medium. The cells can be seen as having a symmetrical shape with small protruding edges, which were similar to those in a previous study [24]. A filamentous network was also seen in the error image of amplitude (figure 2(b)), and the spacing of the network seemed to be larger than a few hundred nanometres. Since, as shown in figure 2(c), the height of HepG2 cells was around 4 μm, we concluded that the tip was still far from the substrate surface under the indentation.

Figure 3 shows a histogram of E at different positions obtained from the force–distance curve measurement on a central region of the HepG2 cells shown in figure 2. We measured several cells cultured on different days. The average value of E varied from ~0.6 to 1.0 kPa.

Figure 4 shows a force–distance curve of HepG2 cells obtained on the stress relaxation experiment. In this case, the tip approached the cell until the loading force attained $F_M \sim 0.95$ nN (red/upper dots). As the tip pushed the cell

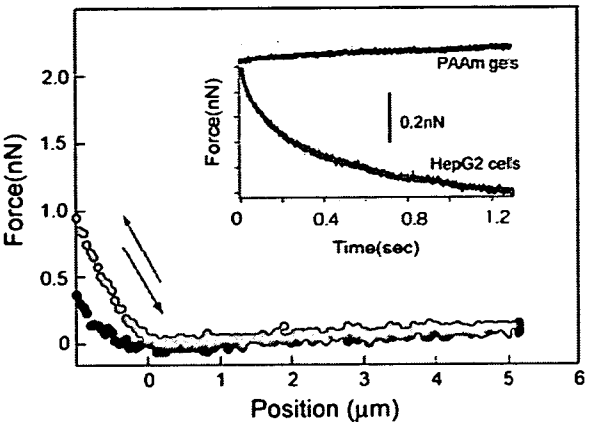

Figure 4. Typical force–distance curve measured in HepG2 cells. Red/upper and blue/lower dots represent curves in the approaching and retracting processes, respectively. The tip approached and pushed the cell surface up to an F_M of 0.95 nN, and the loading force started to decrease due to the viscoelastic properties of the cell. After a T_D of 1.5 s, the tip was retracted from the cell surface, so that the resultant force curves of the approach and retraction broke at the maximum indentation position. The inset shows the time series of the deflection signals observed on the HepG2 and a polyacrylamide (PAAm) gel. The time series of the cantilever deflection signal was smoothed to eliminate noise, including vibration of the cantilever at resonance. The solid (red) line represents the result fitted to a stretched exponential function expressed by equation (2).

surface in the approaching process, no abrupt decrease in the force–distance curve was observed. This indicated that no destruction of the cell membrane [25, 26] took place in this process. While keeping the cantilever base displacement at a constant position, the loading force was found to decay nonlinearly, as shown in the inset of figure 4. It was noted that such a decay was no longer observed using a poly(acrylamide) (PAAm) gel substrate prepared at a standard concentration of monomer and crosslinker [27], which was much harder than the cells. Although the loading force for a PAAm gel sample slightly increased with time, as shown in the inset of figure 4, this was probably due to a drift in the cantilever and/or a relative change of distance between the sample and the AFM system. Therefore, we conclude that the decay of loading force observed on the HepG2 cells should be attributed to their viscoelastic properties, and estimated that the relaxation process appeared at an early stage of <1.5 s.

In previous studies [5, 7], a characteristic adhesion has been observed as the scan rate increases, showing that the adhesive interaction between the tip and the cell surface strongly depends on the experimental conditions of the force–distance curve measurement. In the retracting process shown in figure 4 (blue/lower dots), such an adhesion was invisibly small, and thus it was considered that the relaxation of the loading force was not related to the change in the interaction between the tip and the cell surface. Also, in the retracting curve, the detaching point was almost the same as the contact point in the approaching curve. This means that the force-induced irreversible deformation, i.e., cell plasticity [15], was not apparently occurring at a loading force of ~1 nN. Moreover, no marked difference between the approaching and retracting force curves was observed at a position far from the cell surface, i.e., in non-contact regions, showing that the

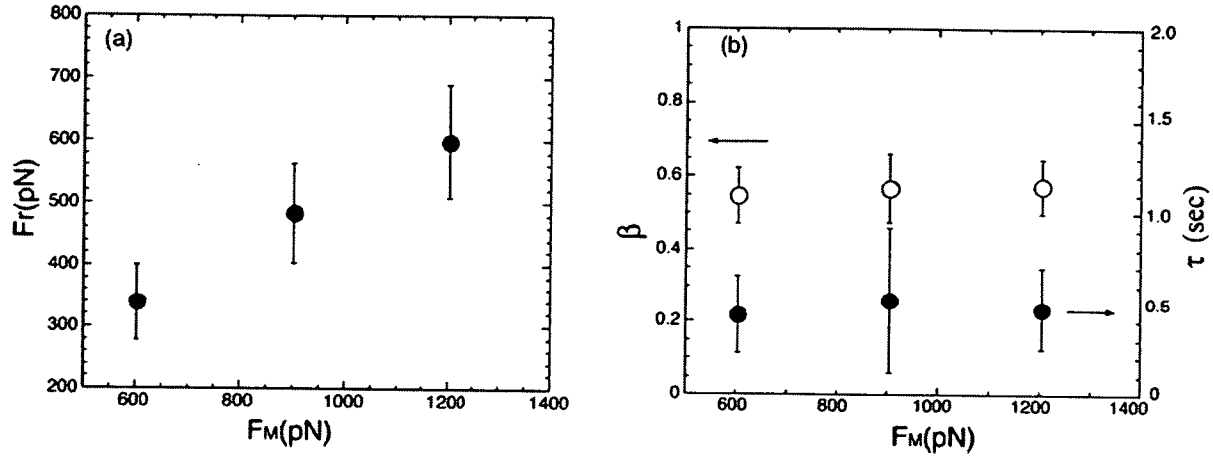

Figure 5. (a) F_r and (b) β and τ which were estimated from a stretched exponential function as a function of F_M, measured on HepG2 cells.

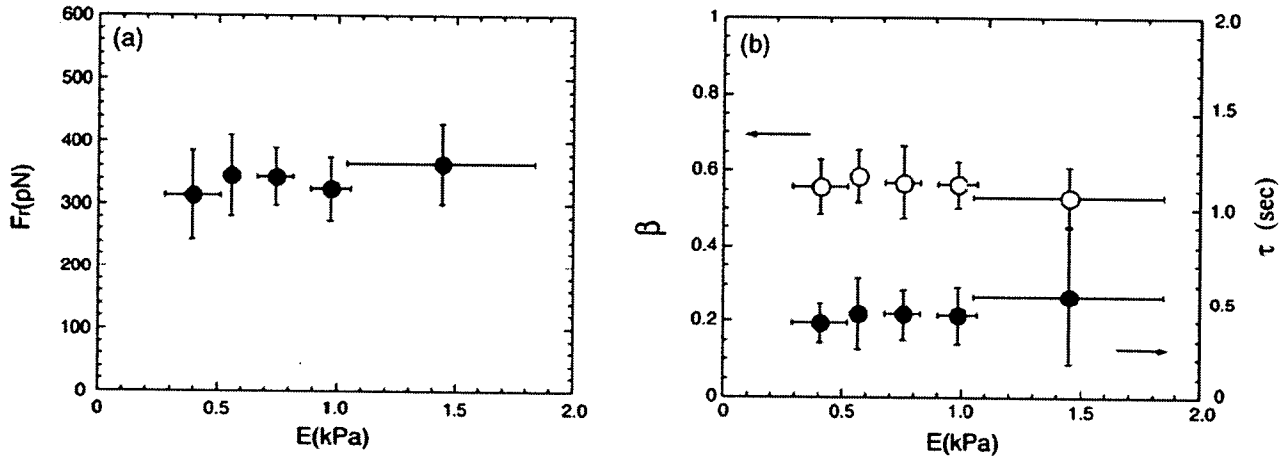

Figure 6. (a) F_r and (b) β and τ which were estimated from a stretched exponential function as a function of E, measured with $F_M = 600$ pN on HepG2 cells.

hydrodynamic drag force [8, 20] due to the liquid environment was negligibly small in the present scan rate.

The observed relaxation of loading force could not be fitted to a single exponential function. Here, we employed a stretched exponential function known as the Kohlrausch–Williams–Watts (KWW) function [28, 29], which is empirically employed to represent the dispersion processes of the system. The functional form is expressed by

$$F(t) = F_r \exp\left[-\left(\frac{t}{\tau}\right)^{\beta}\right] + F_\infty, \qquad (2)$$

where F_r is the relaxation amplitude, F_∞ is the final state of the relaxation process, and τ is the characteristic relaxation time. β is the stretching exponent, with values between zero and unity. The numerical curve fitting equation (2) to the experimental data was derived using IgorPro software (WaveMetrics, Portland, OR, USA). We found that the relaxation of loading force could be well fitted to the stretched exponential function, and an example of the fitted result is shown in the inset of figure 4, as a solid (red) line.

Figure 5 shows the fitted results of relaxation parameters F_r, τ and β as a function of F_M. As shown in figure 5(a), F_r increased with increasing F_M. On the other hand, as shown in figure 5(b), τ and β were independent of F_M, which were ~0.5 s and 0.4–0.6, respectively. The latter indicated that the relaxation observed in HepG2 cells consisted of multiple relaxation processes.

Recent force–modulation experiments [13, 14] have shown that the viscoelastic properties of cells exhibit weak power-law behaviour, 'soft-glassy rheology', over a wide range of frequencies from 0.1 to 100 Hz. In glassy systems, the relaxation curve of viscoelastic properties with $\beta < 1$ has been commonly observed [29]. Therefore the result shown in figure 5(b) suggests that the stress relaxation of HepG2 cells behaves like that in a glassy system.

Figure 6 shows the relation between E and the relaxation parameters such as F_r, τ and β, which was measured with $F_M = 0.6$ nN. Interestingly, the relaxation parameters were almost independent of E. According to the modified Hertz model [23], the diameter of the contact area between the AFM tip and the cell surface, d_{cone}, for the conical indenter is expressed as $d_{cone} = 4\delta \tan\alpha/\pi$. In the present case, for $\alpha = 17.5°$ [18] and $F_M = 0.6$ nN, d_{cone} was estimated to be ~0.6 μm, as E was assumed to be 1 kPa. By comparing the estimated value of the contact area with the cell image

shown in figure 2(b), it is considered that the loading force was intensively applied to one or a few filaments.

It is known that the local elastic properties measured by the indentation are strongly related to filamentous structures formed inside cells. Previous AFM studies with chemical doping suggest that the measured Young's modulus, in a local region, is mainly attributed to actin filaments rather than microtubules and intermediate filaments [9, 15]. These results indicate that the relaxation phenomena observed in the present study may be less correlated with that of the actin filaments than with other filamentous polymers of the cytoskeleton, and/or that various intracellular materials might play a major role in the fast relaxation process.

4. Conclusion

The stress relaxation technique with AFM was employed to measure the viscoelastic properties of HepG2 cells. The decay (relaxation process) of force applied to the cell surface was clearly observed, and the relaxation could be well fitted to a stretched exponential function (KWW function). We found that the relaxation amplitude F_r increased with the trigger force F_M, while the relaxation time τ and the stretching exponent parameter β were independent of F_M. The value of 0.4–0.6 for β implies that the observed relaxation process exhibited multiple relaxation processes like a glassy system. Moreover, we found no obvious dependence between the characteristic relaxation process and the Young's modulus, implying that the observed relaxation process may be related not to the specific actin filaments, but to various other intracellular materials.

Acknowledgment

We thank Dr A Toda (Olympus Co.) for kindly providing us with the small cantilevers, 'BioLever mini' BL-AC40TS.

References

[1] Jena B P and Horber J K H (ed) 2002 Atomic force microscopy in cell biology *Methods in Cell Biology* vol 68 (New York: Academic)
[2] Morris V J, Kirby A R and Gunning A P 1999 *Atomic Force Microscopy for Biologists* (London: Imperial College Press)
[3] Tao N J, Lindsay S M and Lees S 1992 *Biophys. J.* **63** 1165
[4] Weisenhorn A L, Khorsandi M, Kasas S, Gotzos V and Butt H J 1993 *Nanotechnology* **4** 106
[5] Hoh J H and Schoenenberger C A 1994 *J. Cell Sci.* **107** 1105
[6] Rotsch C, Jacobson K and Radmacher M 1999 *Proc. Natl Acad. Sci. USA* **96** 921
[7] A-Hassan E, Heinz W F, Antonik M D, D'Costa N P, Nageswaran S, Schoenenberger C A and Hoh J H 1998 *Biophys. J.* **74** 1564
[8] Radmacher M, Fritz M, Kacher C M, Cleveland J P and Hansma P K 1996 *Biophys. J.* **70** 556
[9] Rotsch C and Radmacher M 2000 *Biophys. J.* **78** 520
[10] Radmacher M, Tillmann R W, Fritz M and Gaub H E 1992 *Science* **257** 1900
[11] Radmacher M, Tillmann R W and Gaub H E 1993 *Biophys. J.* **64** 735
[12] Mahaffy R E, Shih C K, MacKintosh F C and Kas J 2000 *Phys. Rev. Lett.* **85** 880
[13] Alcaraz J, Buscemi L, Grabulosa M, Trepat X, Fabry B, Farre R and Navajas D 2003 *Biophys. J.* **84** 2071
[14] Smith B A, Tolloczko B, Martin J G and Grutter P 2005 *Biophys. J.* **88** 2994
[15] Wu H W, Kuhn T and Moy V T 1998 *Scanning* **20** 389
[16] Darling E M, Zauscher S and Guilak F 2006 *Osteoarthritis Cartilage* **14** 571
[17] Morris K M, Aden D P, Knowles B B and Colton H R 1982 *J. Clin. Invest.* **70** 906
[18] Toda A, Kitazawa M and Yagi A 2004 *Japan. J. Appl. Phys.* **43** 4671
[19] Bippes C A, Humphris A D L, Stark M, Muller D J and Janovjak H 2006 *Eur. Biophys. J* **35** 287
[20] Alcaraz J, Buscemi L, Puig-De-Morales M, Colchero J, Baro A and Navajas D 2002 *Langmuir* **18** 716
[21] Hutter J L and Bechhoefer J 1993 *Rev. Sci. Instrum.* **64** 1868
[22] Dimitriadis E K, Horkay F, Maresca J, Kachar B and Chadwick R S 2002 *Biophys. J.* **82** 2798
[23] Sneddon I N 1965 *Int. J. Eng. Sci.* **3** 47
[24] Yin C, Liao K, Mao H Q, Leong K W, Zhuo R X and Chan V 2003 *Biomaterials* **24** 837
[25] Henderson E, Haydon P G and Sakaguchi D S 1992 *Science* **257** 1944
[26] Hategan A, Law R, Kahn S and Discher D E 2003 *Biophys. J.* **85** 2746
[27] Okajima T, Harada I, Nishio K and Hirotsu S 2002 *J. Chem. Phys.* **116** 9068
[28] Williams G and Watts D C 1970 *Trans. Faraday Soc.* **66** 80
[29] Lee A and Lichtenhan J D 1998 *Macromolecules* **31** 4970

Effect of Honeycomb-Patterned Surface Topography on the Adhesion and Signal Transduction of Porcine Aortic Endothelial Cells

S. Yamamoto,*,†,‡ M. Tanaka,‡,§ H. Sunami,†,‡ E. Ito,‡ S. Yamashita,‡ Y. Morita,† and M. Shimomura‡,§

Creative Research Initiative "Sousei" (CRIS), Hokkaido University, N21 W10 Kita-ku, Sapporo 001-0021, Japan, Core Research for Evolutional Science and Technology (CREST), Japan Science and Technology Agency (JST), Honchou 4-1-8, Kawaguchi 332-0012, Japan, and Nanotechnology Research Center, Research Institute for Electronic Science, Hokkaido University, N21 W10 Kita-ku, Sapporo 001-0021, Japan

Received February 6, 2007. In Final Form: May 9, 2007

Surface topography has vital roles in cellular response. Here, to investigate the mechanism behind cellular response to surface topography, we prepared honeycomb (HC)-patterned films from poly(ϵ-caprolactone) (PCL) with micropatterned surface topography by casting a polymer solution of water-immiscible solvent under high humidity. We characterized the adsorption of fibronectin (Fn) on the film using atomic force microscopy (AFM) and confocal laser scanning microscopy (CLSM). The response of porcine aortic endothelial cells (PAECs) to adsorbed Fn molecules onto HC-patterned films was observed by immunofluorescence labeling of vinculin and the actin fiber of PAECs cultured for 1 and 72 h in serum-free medium. The expression of focal adhesion kinase autophosphorylated at the tyrosine residue (pFAK) at 1 h culture was determined using an immunoprecipitation method. Fn adsorbed selectively around the pore edges to form ring-shaped aggregates. The immunostaining results revealed that PAECs adhered to the HC-patterned films at focal contact points localized around pore peripheries. These points correspond to adsorption sites of Fn. The expression of pFAK after 1 h on the HC-patterned film was 3 times higher than that on a corresponding flat film, indicating that the signaling mediated by the binding between Fn and the integrin receptor was more highly activated on the HC-patterned film. These results suggest that the cellular response to HC-patterned films (e.g., adhesion pattern and phosphorylation of FAK) originates from the regularly aligned adsorption pattern of Fn determined by the pore structure of the film.

Introduction

Tissue engineering aims to restore, maintain, or improve complex human tissue function. This has come about by combining natural or synthetic substrates with cellular components.[1] Since the original report that cells react to surfaces,[2] cellular response to material surfaces has been an intriguing topic in tissue engineering. Research has documented that surface properties such as chemistry, charge, rigidity, and topography play vital roles in cellular behavior, such as adhesion, spreading, migration, proliferation, and differentiation. Recently, polymer substrates for cell-culture with geometric subcellular patterns have been fabricated by various fabrication methods and have been extensively used to investigate how cells respond to surface topography.[3−11] We reported that honeycomb (HC)-patterned porous polymer films can be prepared by casting functionally selected polymer dissolved in a water-immiscible solvent under high humidity.[12,13] This technology was adopted for biological applications. Specifically, the morphology and hence the function of hepatocytes,[14,15] cardiac myocytes (CMs),[16] and neural progenitor cells[17] were all controlled by manipulating the size and shape of the micropores on the HC-patterned films. Although the effects of substrate topography on cell function are well documented, the mechanisms behind these interactions remain unresolved.[3]

The interaction between adherent cells and a substrate occurs via cell-surface proteins such as integrin. This is facilitated by a cell adhesion protein such as fibronectin (Fn).[18] When interacting with Fn, integrin receptors form focal adhesion complexes, which act as a "transducer", getting signaling messages across cell membrane. These signaling pathways have been implicated in cell migration, proliferation, and differentiation.[19] The focal

* Corresponding author. Tel: +81-11-706-9255. Fax: +81-11-706-9291. E-mail: syama@cris.hokudai.ac.jp.
† (CRIS), Hokkaido University.
‡ Japan Science and Technology Agency.
§ Research Institute for Electronic Science, Hokkaido University.

(1) Langer, R.; Vacanti, J. P. *Science* **1993**, *260*, 920−926.
(2) Carrel, A.; Burrows, M. *J. Exp. Med.* **1911**, *13*, 571−575.
(3) den Braber, E. T.; de Ruijter, J. E.; Grinsel, L. A.; von Recum, A. F.; Jansen, J. A. *J. Biomed. Mater. Res.* **1998**, *40*, 291−300.
(4) Flemming, R. G.; Murphy, C. J.; Abrams, G. A.; Goodman, S. L.; Nealey, P. F. *Biomaterials* **1999**, *20*, 573−588.
(5) Curtis, A.; Riehle, R. *Phys. Med. Biol.* **2001**, *46*, R47−R65.
(6) Teixeira, A. I.; Abrams, G. A.; Bertics, P. J.; Murphy, C. J.; Nealey, P. F. *J. Cell Sci.* **2003**, *116*, 1881−1892.
(7) Motlagh, D.; Hartman, T. J.; Desai, T. A.; Russell, B. *J. Biomed. Mater. Res.* **2003**, *67A*, 148−157.
(8) Dalby, M. J.; Childs, S.; Riehle, M. O.; Johnstone, H. J. H; Affrossman, S.; Curtis, A. S. G. *Biomaterials* **2003**, *24*, 927−935.
(9) Arnold, M.; Cavalcanti-Adam, A. E.; Glass, R.; Blümmel, J.; Eck, W.; Kantlehner, M.; Kessler, H.; Spatz, J. P. *ChemPhysChem* **2004**, *5*, 383−388.
(10) Dalby, M. J.; Riehle, M. O.; Sutherland, D. S.; Agheli, H.; Gurtis, A. S. G. *J. Biomed. Mater. Res.* **2004**, *69A*, 314−322.
(11) Berry, C. C.; Dalby, M. J.; McCloy, D.; Affrossman, S. *Biomaterials* **2005**, *26*, 4985−4992.
(12) Maruyama, N.; Koito, T.; Nishida, J.; Sawadaishi, T.; Gieren, X.; Ijiro, K.; Karthaus, O.; Shimomura, M. *Thin Solid Films* **1998**, *854*, 327−329.
(13) Tanaka, M.; Takebayashi, M.; Miyama, M.; Nishida, J.; Schimomura, M. *Bio-Med. Mater. Eng.* **2004**, *14*, 439−446.
(14) Sato, K.; Hasebe, K.; Tanaka, M.; Takebayashi, M.; Nischikawa, M.; Schimomura, M.; Kawai, T.; Matsushita, M.; Todo, S. *Int. J. Nanosci.* **2002**, *1*, 689−693.
(15) Tanaka, M.; Nishikawa, K.; Okubo, H.; Kamachi, H.; Kawai, T.; Matsushita, M.; Todo, S.; Schimomura, M. *Colloids Surf., A* **2006**, *464*, 284−285.
(16) Nishikawa, T.; Nonomura, M.; Arai, K.; Hayashi, J.; Sawadaishi, T.; Nishiura, Y.; Hara, M.; Shimomura, M. *Langmuir* **2003**, *19*, 6193−6201.
(17) Tsuruma, A.; Tanaka, M.; Fukushima, N.; Shimomura, M. *e-J. Surf. Sci. Nanotechnol.* **2005**, *3*, 159−164.
(18) Hynes, R. O. *Fibronectin*; Springer: New York, 1990; p 546.

10.1021/la7003326 CCC: $37.00
Published on Web 06/19/2007

adhesion complexes contain structural proteins (such as vinculin, talin, and α-actinin), signal-transduction molecules, and trigger-signaling pathways. A typical example of signal-transduction molecules is focal adhesion kinase (FAK).[20] FAKs localized in a focal adhesion complex are autophosphorylated at their tyrosine residue 397, creating a high-affinity binding site for various signal-transduction proteins and then phosphorylating these proteins. Thus, extracellular stimuli are translated downstream, directing the adhesion, survival, or proliferation of endothelial cells (ECs).[20] The adhesion, proliferation or extra cellular matrix production of ECs are influenced by the surface topography and composition of the substrate surface; understandably, the signaling pathways mediated by the interaction between Fn and integrin may be affected by the surface topography and composition.[20−27] Previously, we demonstrated that the adhesion, proliferation, and extracellular matrix (ECM) production of porcine aortic endothelial cells (PAECs) are influenced by HC-patterned films.[28] Hypothetically, pre-adsorption of Fn on HC-patterned film will influence these cellular activities.

In a previous study,[29] we investigated the effect of HC-patterning on the adsorption of Fn. Furthermore, we investigated the mechanisms involved in the response of PAECs and CMs to HC-patterned surfaces. We observed Fn aggregation around the peripheral margins of HC micropores. However, due to the difference in Fn adsorption characteristics in culture medium and phosphate-buffered saline (PBS) (Vroman effect[30]), correlations between the location of the Fn aggregates and the focal adhesion patterns of PAECs and CMs were inconclusive.

The present work investigates the mechanism behind PAECs response to HC-patterned surface. It is widely accepted that both protein precoating and substrate surface characteristics are important independently. Indeed, cell adhesion, proliferation, and ultimately ECM production have all been shown to depend on their parameters.[28] It is therefore necessary to understand the coupled effect of protein adsorption and surface characteristics and highlight key molecules involved. We expect that the differences in substrate surfaces will govern protein adsorption characteristics (e.g., distribution) and, in turn, influence cellular behavior via focal adhesion formation.

Experimental Section

Film Preparation. Poly(ε-caprolactone) (PCL) and an amphiphilic copolymer (CAP) of dodecylamide and ω-carboxyhexylacrylamide (Figure 1) were used to fabricate both the flat and HC-patterned films. PCL (Wako, Japan) has molecular weights between 70 and 100 kDa. The CAP powder was synthesized as previously reported.[31]

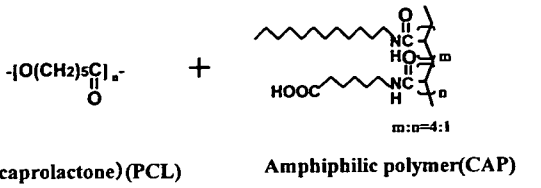

Poly(ε-caprolactone) (PCL) **Amphiphilic polymer(CAP)**

PCL:CAP=10:1(wt%)

Figure 1. Chemical structures of PCL and CAP, both of which were used to manufacture the HC-patterned films.

The HC-patterned films were fabricated on a 15 mm-diameter cover glass (Matsunami Glass Industry, Japan) by casting a 10:1 ratio (w/w) of PCL and CAP, respectively, in chloroform as previously described.[12,13] The flat films were prepared by spin-coating 150 μL of the same polymer solution at a chloroform concentration of 10 mg/mL onto a cover glass at approximately 30% humidity and 21 ± 1 °C using a commercially available spin-coater (1H-7D, Mikasa, Japan).

The water used throughout the present study was purified using a Millipore system (Milli-Q, Millipore). The organic solvents and chemicals employed were all commercially available and were used according to the manufacturer's instructions.

Adsorbed Fn Assay. The quantities of Fn adsorbed onto the films were determined for different Fn concentrations and incubation times up to 50 h using bicinconic acid (BCA), a protein assay reagent (Pierce, IL).[32] Fn was sourced from bovine plasma (lyophilized from 0.05 M tris-buffer saline, pH 7.5) purchased from Sigma (Munich, Germany). HC-patterned and flat films were transferred to a 24-well tissue culture plate (Iwaki, Japan). A 200 μL portion of Fn/PBS solution (concentrations between 0 and 6000 μg/mL) was added into each well. Subsequently, the films in the plates were incubated for up to 50 h under standard culture conditions (37 °C and 5% CO_2). After incubation, the Fn/PBS solutions were removed from the wells, and then the films were washed two times in PBS. The reaction started at 37 °C after 200 μL of a working reagent was added to each well. After incubation for 2 h, 160 μL of the Fn solution was transferred into a 96-well plate for measuring absorbance at 590 nm by a microplate reader (Biotrak II, Biochrom, Ltd., U.K.)

Atomic Force Microscopy (AFM), Confocal Laser Scanning Microscopy (CLSM), and Scanning Electron Microscopy (SEM) Measurements. Tapping-mode AFM imaging was performed under ambient conditions using a Digital Instrument Nanoscope IIIa Multimode system (Digital Instruments, Santa Barbara, CA) equipped with silicon tips. The tips had a resonance frequency of ~300 kHz and a force constant of 14 N/m. The scan rate was 0.1−0.2 Hz, and the proportional and integral gains were set in the range of 2−10. The cell cytoskeletons were imaged using a CLSM apparatus (FLUOVIEW FV300, Olympus, Japan). For preparing specimens, the HC and flat films were incubated separately in 200 μL aliquots of Fn dissolved in PBS at a concentration of 240 μg/mL for 48 h under standard culture conditions. The Fn adsorbed films were then gently washed with PBS, fixed with 10% formaldehyde (Wako, Japan) for 10 min at room temperature, permeabilized in PBS containing 1% normal goat serum and 0.1% Triton X-100 for 30 min in order to pin adsorbed Fn and prevent nonspecific adsorption of antibodies, and then incubated for 1 h with anti-Fn antibody (diluted 1:500; Sigma, Taufkirchen, Germany). After being rinsed with water, the films were treated with fluorescein isothiocyanate (FITC)-conjugated anti-rabbit IgG antibody (diluted 1:2000, Cappel Laboratories, Durham, NC). For SEM imaging, the HC-patterned films were sputter-coated with Pt−Pd using a commercially available unit (Hitachi E1030, Hitachi, Japan). SEM images were obtained using a Hitachi S-3500N SEM (Hitachi, Japan) at an acceleration voltage of 15 kV.

Culture of PAECs. Frozen PAECs (CSC Certificate, Dainippon Pharmaceutical Co., Ltd., Japan) were thawed at 37 °C and

(19) *Molecular Biology of the Cell*, 4th ed.; Alberts, B., Johnson, A., Lewis, J., Raff, M., Roberts, K., Walter, P., Eds.; Newton Press: Tokyo, 2004.
(20) Schaller, M. D.; Borgman, C. A.; Cobb, B. S.; Vines, R. R.; Reynolds, A. B.; Parsons, J. T. *Proc. Natl. Acad. Sci. U.S.A.* **1992**, *89*, 5192−5196.
(21) Iuliano, D. J.; Saavedra, S. S.; Truskey, G. A. *J. Biomed. Mater. Res.* **1993**, *27*, 1103−1113.
(22) Brumeister, J. S.; Vrany, J. D.; Reichert, W. M.; Truskey, G. A. *J. Biomed. Mater. Res.* **1996**, *30*, 13−22.
(23) Koenig, A. L.; Gambillara, V.; Grainger, D. W. *J. Biomed. Mater. Res.* **2003**, *64A*, 20−37.
(24) Sanborn, S. L.; Murugesan, G.; Marchant, R. E.; Kottke-Marchant, K. *Biomaterials* **2002**, *23*, 1−8.
(25) Sagnella, S. M.; Kligman, F.; Anderson, E. H.; King, J. E.; Murugesan, G.; Marchant, R. E.; Kottke-Marchant, K. *Biomaterials* **2004**, *25*, 1249−1259.
(26) Chen, Y. M.; Shiraishi, N.; Satokawa, H.; Kakugo, A.; Narita, T.; Gong, J. P.; Osada, Y.; Yamamoto, K.; Ando, J. *Biomaterials* **2005**, *26*, 4588−4596.
(27) Boura, C.; Muller, S.; Vautier, D.; Dumasa, D.; Schaaf, P.; Voegel, J. C.; Stoltz, J. F.; Menu, P. *Biomaterials* **2005**, *26*, 4568−4575.
(28) Tanaka, M.; Takayama, A.; Ito, E.; Sunami, H.; Yamamoto, S.; Shimomura, M. *J. Nanosci. Nanotechnol.* **2007**, *7*, 763−772.
(29) Yamamoto, S.; Tanaka, M.; Sunami, H.; Arai, K.; Takayama, A.; Yamashita, S.; Morita, Y.; Shimomura, M. *Surf. Sci.* **2006**, *600*, 3785−3791.
(30) Vroman, L.; Adams, A. L.; Fisher, G. C.; Munoz, P. C. *Blood* **1980**, *55*, 156−159.
(31) Nishimura, S.; Yamada, K. *J. Am. Chem. Soc.* **1997**, *119*, 10555−10556.
(32) Pernodet, N.; Rafailovich, M.; Sokolov, J.; Xu, D.; Yang, N.-L.; McLeod, K. J. *Biomed. Mater. Res.* **2003**, *64A*, 684−692.

resuspended into a culture medium (Dulbecco's modified Eagle's minimal essential medium, Sigma, Taufkirchen, Germany) supplemented with 10% FBS (Thermo Trace, Australia), 100 unit/mL penicillin streptomycin (GIBCO, Carlsbad, CA). Following their initial culture, the PAECs at passages 6−8 were resuspended in serum-free medium for up to 96 h. Subsequently, the cells were plated onto the Fn-coated HC and flat films on cover glasses at a density of 1.5×10^4 cells/cm^2 and cultured in the serum-free culture medium under standard culture conditions for 1 and 72 h, respectively.

Immunostaining of PAEC for Vinculin, Actin Fiber, Phosphorylated FAK (pFAK), and Nuclei. To visualize the focal adhesion, vinculin, actin fiber, and pFAK were stained at 1 and 72 h using an established method. After washing with PBS, the cells were fixed with 10% formaldehyde (Wako, Japan) for 10 min at 20 °C and washed twice with PBS. The cells were then permeated with 1% Triton X-100 (MP Biomedicals, Solon, OH) in PBS solution for 5 min at 20 °C. Vinculin and pFAK were stained using primary antibodies (mouse anti-vinculin monoclonal antibody, Chemicon, Temecula, CA) and unconjugated rabbit anti-FAK [pY^{397}] phosphospecific antibody from Biosource (Camarillo, CA) for each antigen and using fluorescence-labeled secondary antibodies (Alexa Fluor 546 goat anti-mouse IgG, Alexa Fluor 488 phalloidin, Alexa Fluor 488 goat anti-rabbit IgG, Molecular Probes, Carlsbad, CA). Actin fibers were stained with rhodamine-conjugated phalloidin (Molecular Probes, Carlsbad, CA). The cell nuclei were stained with DAPI (Molecular Probes, Carlsbad, CA). The stained cells were rinsed four times with PBS, and subsequently immersed for 1 h after the fourth rinse. All specimens were placed on glass slides, then covered with glass coverslips, and sealed with nail polish. The specimens were imaged using the CLSM (FV-300, Olympus, Japan).

Quantification of pFAK by Immunoprecipitation. A buffer solution for immunoprecipitation, RIPAB, was prepared by mixing 10 mM Tris-HCl (pH 7.5)/150 mM NaCl/1% Nonidet P-40/0.5% sodium deoxycholate/0.1% sodium dodecyl sulfate and Protease Inhibitor Cocktail Set III (Calbiochem; San Diego, CA 1/100). The RIPAB was then mixed with ProteinG-Sepharose P-3296 (Sigma, Taufkirchen, Germany) at 1:1 vol %. ProteinG-Sepharose with anti-FAK was prepared by mixing ProteinG-Sepharose P-3296 with anti-FAK (BD, San Jose, CA) at 4 °C for 6 h. PAECs cultured for 1 h were lysed in RIPAB for 20 min on ice. The lysates were centrifuged at 15 000g for 20 min at 4 °C, and the total cell protein concentration was measured using a BCA kit (Pierce, Rockford, IL). Samples obtained from lysates were mixed with the anti-FAK/ProteinG-Sepharose and incubated for 13 h at 4 °C. A 90 vol % portion of lysates and obtained immunoprecipitates was loaded onto 7% polyacrylamide gel for electrophoresis (MiniPROTEAN 3 Cell, BIO-RAD, Hercules, CA). After protein migration, the gels were blotted onto a polyvinylidene fluoride membrane (immune-Blot PVDF membrane, BIO-RAD, Hercules, CA). The membranes of both the lysate and the immunoprecipitate samples were stained with mouse anti-FAK and rabbit anti-pFAK antibody in 1% BSA/TBS-T (1:500 Biosource, Camarillo, CA), respectively, and then with fluorescence-labeled secondary antibodies (horseradish peroxidase (HRP)−mouse IgG in TBS-T 1:500, HRP−rabbit IgG in TBS-T, Biosource, Camarillo, CA). The expression of pFAK was detected by chemiluminescence using ECL reagents (Amersham) (Fujifilm LAS-3000 mini, Japan).

Results and Discussion

HC Structure. An SEM micrograph of the HC-patterned film (Figure 2a) reveals a well-aligned hexagonal lattice of the PCL materials. The tilted and side-view images (Figure 2b,c) of the same film demonstrate the double-layered structure in which two hexagonal lattices were connected vertically by columns at the vertex of hexagons. Figure 2d shows a schematic model of this double-layered structure.

Amount and Structure of Fn Adsorption. The amount of Fn adsorbed on both the HC and flat films was measured as a function of both incubation time and Fn-coating concentration

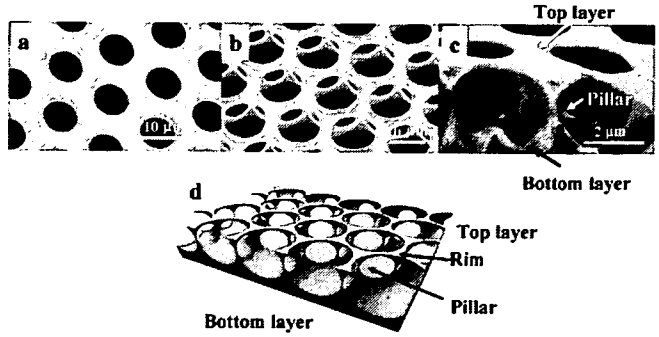

Figure 2. SEM images of the HC-patterned film: (a) top view, (b) tilted view, and (c) side view. (d) Schematic of the double-layered structure of the film.

and was quantified using a total adsorbed protein assay. For both films, the amount of Fn adsorbed increased linearly with incubation time, reaching a plateau at 1 h. Upon increasing Fn-coating concentration up to 50 μg/mL, the amount of Fn on the flat film increased drastically and then saturated when the Fn-coating concentration reached 600 μg/mL (Figure 3). Although the adsorption rate on the HC-patterned films was similar to that on the flat films, the amount of Fn adsorbed on HC-patterned films was approximately twice that on the flat film. Indeed, the amount of Fn adsorbed at saturation on a flat film was 0.52 μg, while that on an HC-patterned film was 0.91 μg. The surface density at saturation on a flat film was about 0.4 μg/cm^2. This estimation is based on the calculated surface area of the flat films (1.32 cm^2) and on the adsorbed amount (0.52 μg). This is in good agreement with the amount of Fn required for monolayer saturation, namely, 0.32 μg/cm^2.[33−36] The surface area of the HC-patterned film was not measured in the present work. This is essentially difficult with currently available techniques such as the Brunauer−Emmett−Teller (BET) method due to the low surface area of the HC-patterned films. Further experiments should endeavor to determine the exact surface area of the porous film, perhaps by BET. We estimated the surface area of HC-patterned films from the porosity of HC-patterned films (the ratio of pore area to total surface area of a top sheet) of about 0.5 and the double-layer structure (shown in Figure 2). Because of the double-layer structure, the proteins are able to adsorb on the top, inner (rear sides of the top layer), and bottom surface of the HC-patterned film. Indeed, the fluorescence profile of the HC-patterned films demonstrated that Fn molecules adsorbed onto the top, inner, and bottom surfaces of the HC films (Figure 4d−f). The surface area available for Fn adsorption of a top surface is half that of a flat film, as the porosity of HC-patterned films is 0.5. However, Fn molecules adsorb on the rear side of the top layer. This means that the surface area for Fn adsorption of a top layer is equal to that of a flat film. In addition, Fn molecules adsorb on the bottom surface, the area of which is almost equal to that of a flat film. Thus, the HC surface area, or at least the area available for protein adsorption, is approximately twice that of a flat film. On the basis of the estimated surface area of an HC-patterned film (twice the surface area of a flat film) and of the adsorbed amount (0.91 μg), the surface density of Fn on an HC-patterned film is equal to that on a flat film. The total adsorbed protein assay indicates a monolayer-level adsorption of Fn on both the flat and HC-patterned films.

(33) Garcia, A. G.; Vega, M. D.; Boettinger, D. *Mol. Biol. Cell* **1999**, *10*, 785−798.
(34) Garcia, A. G.; Boettinger, D. *Biomaterials* **1999**, *20*, 2427−2433.
(35) Grinnel, F.; Feld, M. K. *J. Biomed. Mater. Res.* **1981**, *15*, 363−381.
(36) Williams, E. C.; Janmey, P. A.; Ferry, J. D.; Mosher, D. F. *J. Biol. Chem.* **1982**, *257*, 14973−14978.

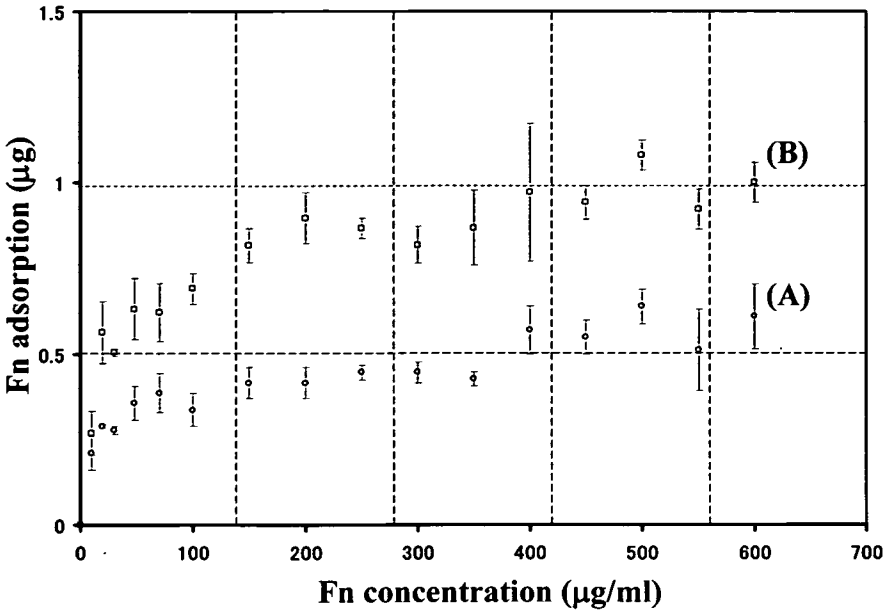

Figure 3. Total amount of Fn adsorbed on (A) a flat film and (B) an HC-patterned film as a function of Fn-coating concentration. Overall averages are represented by the means and standard deviation of three independent experiments for each Fn-coating concentration.

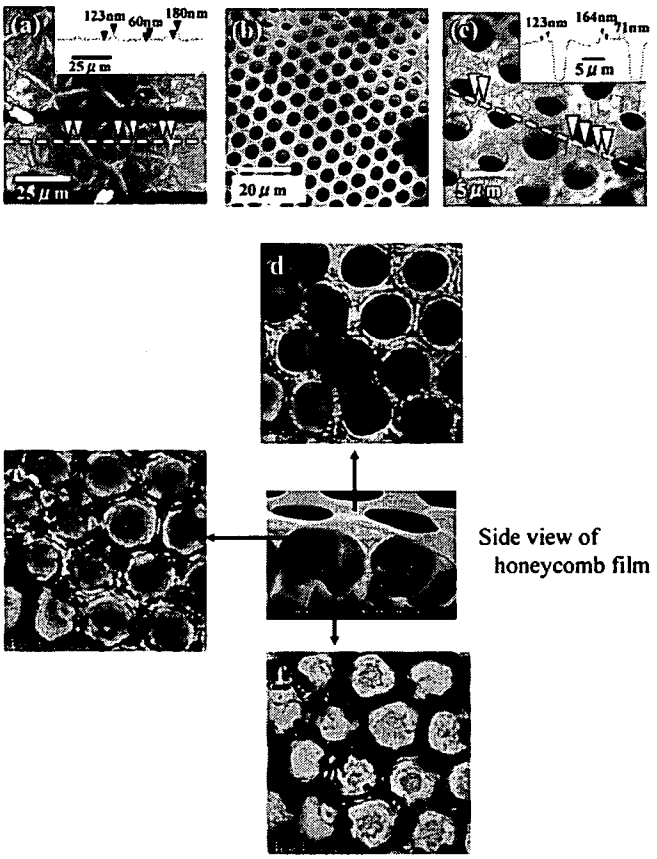

Figure 4. Topographic AFM and CLSM images showing the morphology of Fn adsorbed on an HC-patterned and a flat film after 48-h incubation in a PBS solution of Fn. (a) AFM image of a flat film. Inset is a cross-sectional profile along the dotted line in panel a. (b) AFM image of an HC-patterned film before incubation and (c) after 48-h incubation. Inset in panel c is a cross-sectional profile along the dotted line. CLSM images of the (d) top layer, (e) underside of the top layer, and (f) bottom layer of an HC-patterned film.

Despite the monolayer-level adsorption, Fn distribution was not uniform on either film. Figure 4a shows a representative AFM image of flat films after 48 h of incubation in 240 μg/mL Fn/PBS solution at 37 °C. The surface had an interconnected fibrillar structure. Typical fibrils had 30−50 μm length, 0.5−2 μm width, and 0.05−0.2 μm height (inset in Figure 4a). The fibrillar structure is similar to that of Fn adsorbed onto sulfonated polystyrene films,[32] supporting our supposition that the fibril-like aggregates are pre-coated Fn. The surface of the HC-patterned film after incubation in Fn/PBS solution was completely different from that of a flat film. Before incubation, the surface was flat (Figure 4b). After 48 h of incubation, ring structures about 100 nm high and 1 μm wide were aggregated around the pores (Figure 4c and its inset). The CLSM image of the top surface (Figure 4d) reveals strong ring-like fluorescence along the pore edges, corresponding well to the ring structures evident in the AFM images.

The role of the regular patterns on the protein adsorption has been investigated, and it was demonstrated that protein molecules sense a surface topography, in analogy to what has been observed for cells on subcellular surface topography.[3,32,37] However, the explanation is not straightforward because protein adsorption is a very complex process consisting of several steps. The topographic discontinuities have different surface-free energy and act as a site of preferred protein deposition, creating patterns of proteins along the topographic patterns.[6] Thus, surface-free energy patterns determined by the HC pattern are supposed to have a profound influence on the topologically controlled adsorption of Fn on the HC-patterned film. The recent research supports the argument that the anisotropy of a protein molecule influences the nanometer-scale surface roughness-related adsorption of fibrinogen.[38] The anisotropy of Fn is supposed to have an important role in the pore edge-related adsorption of Fn, too. Protein organization on a patterned surface has been reported for Fn adsorption onto Au/Si micropatterns coated by a sulfonated polystyrene film.[39] Fn was adsorbed on the Si regions of the substrate but was repulsed by the Au domains, resulting in a structure of self-assembling Fn determined by the width of Si

(37) Galli, C.; Collaud Coen, M.; Hauert, R.; Katanaev, V. L.; Wymann, M. P.; Gröning, P.; Schlapbach, L. *Surf. Sci.* **2001**, *474*, L180−L184; *Colloids Surf., B* **2002**, *26*, 255−267.

(38) Rechendorff, K.; Hovgaard, M. B.; Foss, M.; Zhdanov, V. P.; Besenbacher, F. *Langmuir* **2006**, *22*, 10885−10888.

(39) Pernodet, N.; Lenny, S.; John, J.; Miriam, M. *American Physics Society March Meeting 2004*, March 22−26, 2004, Palais des Congress de Montreal: Montreal, Quebec, Canada, 2004; Meeting ID: MAR04, abstract #P9.011.

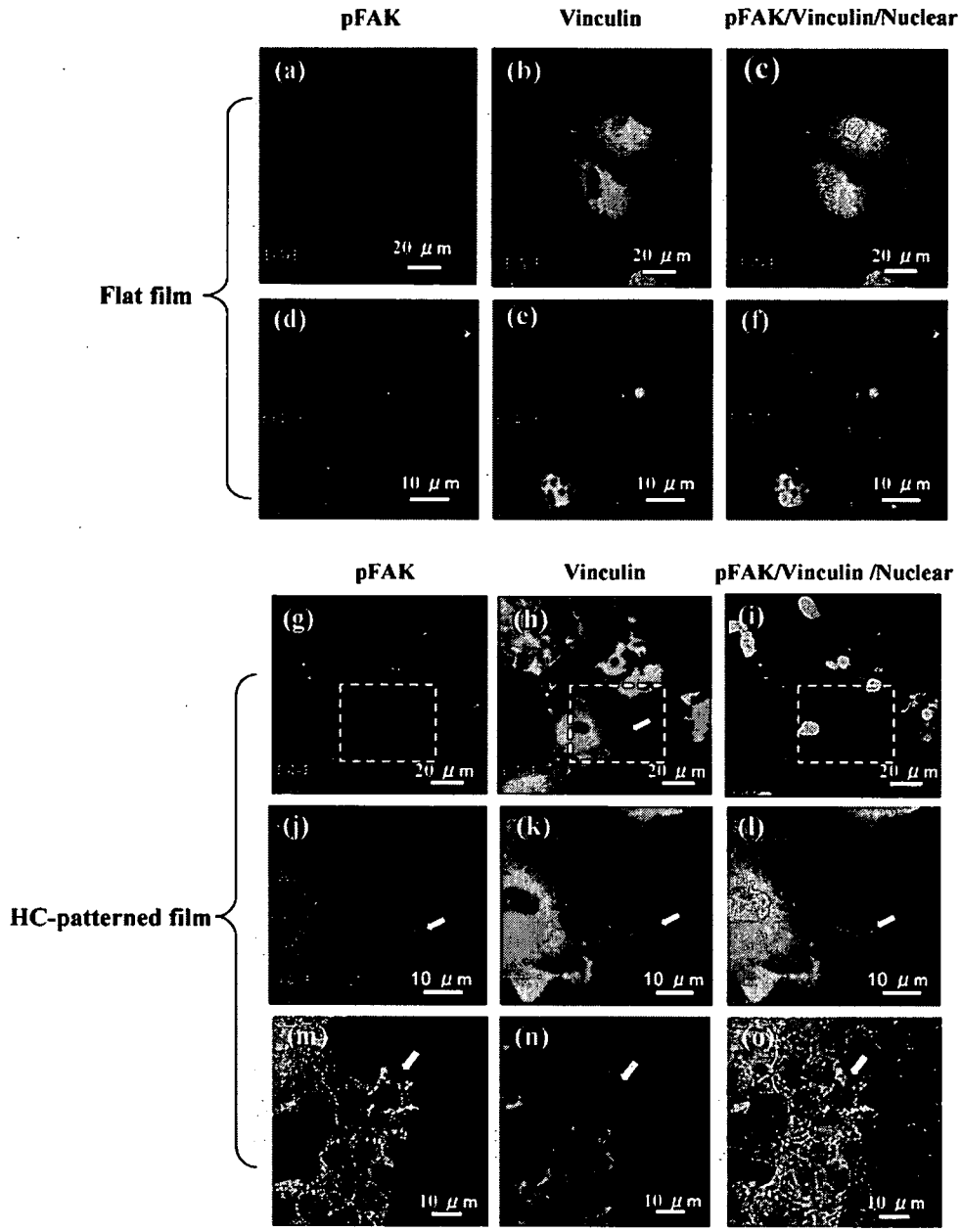

Figure 5. CLSM images of PAECs immunofluorescently stained for vinculin, pFAK, and cell nuclei. PAECs plated on a flat film and an HC-patterned film were cultured and stained for vinculin, pFAK, and cell nuclei at 1 h (a−c,g−i) and 72 h (d−f,m−o). (j−l) Close-up images of enclosed region in panels g−i. Arrows in panel h and circles in panel k indicate locations of focal contact points (vinculin and pFAK) around the periphery of pores. CLSM image shown in panel o is superimposed on a differential interference microscope image of an HC film

domains. The possible mechanism behind this Fn organization on the patterned surface is the balance between the bending energy of Fn and the unfavorable energy of contact with the Au interface. In our current study, the width of a rim of an HC-patterned film on which Fn adsorbed was 2−3 μm. The width of a rim and the size of a pore are comparable to the width of the Si and Au domains of Au/Si micropatterns (several microns to 20 microns). If pores play a role similar to that of Au domains, namely, that Fn does not adsorb, the same mechanism might be responsible for the self-organization of Fn on an HC-patterned film.

Adhesion of PAECs and Expression of pFAK. The expression of vinculin, actin fiber, and pFAK is indicative of a focal adhesion area of PAECs to the ECM. To determine how the adhesion of PAECs is affected by the HC-patterned film, the focal adhesion of PAECs on the Fn-coated HC-patterned film was studied. The difference in the adhesion of PAECs on the HC-patterned and flat films was more pronounced in the cells cultured for a longer time of 72 h.

Expressions of vinculin and pFAK were observed in the perinuclear region of the PAECs cultured for 1 h on the flat film (Figure 5a−c). The perinuclear development of vinculin seemed to be characteristic of ECs at an early culture period. Indeed, perinuclear localization of vinculin has been reported for human pulmonary artery ECs cultured for 1 h.[24] Localization of vinculin and pFAK was also observed at the cell periphery, although pFAK was obscured compared to vinculin (Figure 5a−c). Actin fibers were moderately developed and were associated with spots of vinculin at the cell periphery, indicating the formation of focal contacts at the cell periphery (Figure 6a−c). Vinculin and pFAK of PAECs after a 1 h culture on the HC-patterned film also showed perinuclear localization (Figure 5g−l). Expression of vinculin and pFAK was also observed at the cell periphery. It is worth noting that the expression at the cell periphery has an

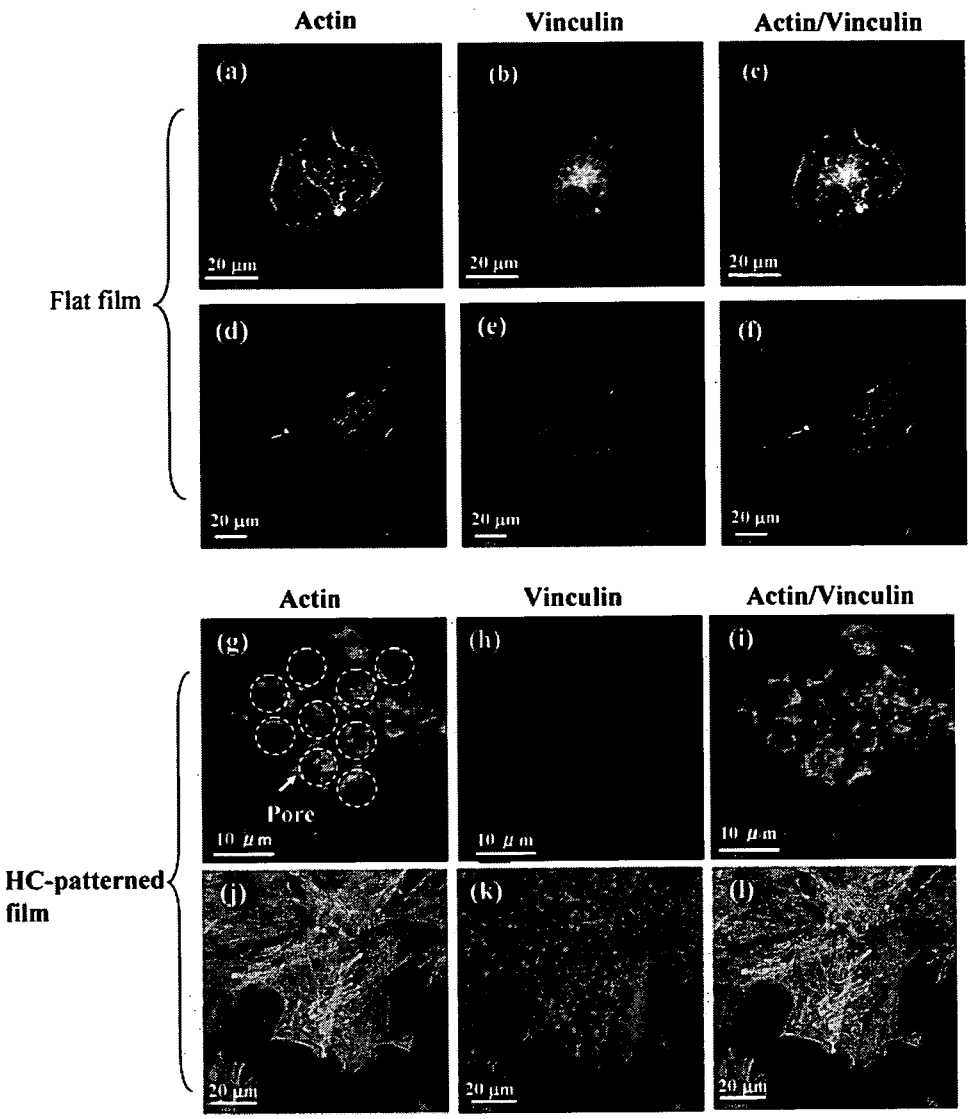

Figure 6. CLSM images of PAECs immunofluorescently stained for actin and vinculin plated on a flat film and an HC-patterned film. PAECs plated on the films were cultured and stained for actin and vinculin at 1 h (a–c,g–i) and 72 h (d–f,j–l). CLSM images shown in panels j–l are superimposed on a differential interference microscope image of an HC film.

HC pattern (Figure 5g–l). This expression indicates that the adhesion of PAECs on the HC-patterned film was localized on the rim of the HC-patterned films. A close inspection of this region (Figure 5g–i) spatially resolved the adhesion of PAECs on the rim (indicated by arrows in Figure 5j–l). These images clearly demonstrate that PAECs after a 1 h culture adhere site-selectively around the periphery of the HC pores, namely, at the edge of the rim. Actin fiber staining was rather diffuse compared to that on the flat film. Localization around HC pores may be seen (Figure 6g). This image indicates the absence of well-defined actin filaments.

The development of actin fibers and focal adhesion complexes was significantly pronounced on both HC and flat films after 72 h of culture (Figures 5d–f,m,n and 6d–f,j–l). PAECs on the flat film clearly developed focal adhesions randomly at the cell periphery that were associated with the well-formed actin fibers (Figures 5d–f and 6d–f). On the other hand, PAECs on the HC-patterned films showed focal adhesion complexes on the rim of the HC-patterned film. Figure 5m–o shows double rings of matured focal adhesion complexes around the HC pores (by white arrows). These images demonstrate that adhesion sites were distributed over the entire cell body with an HC pattern. In addition, they show the location of the focal adhesion at the edge of the rim more clearly than the images shown in Figure 5g–l.

The difference in the focal adhesion pattern and morphology of an actin between the HC-patterned film and the flat film suggests a different signaling pathway and/or efficiency. The extent of FAK phosphorylation on the Fn-coated HC-patterned and flat films was quantified by Western blotting. FAK was recovered from PAEC extracts after a 1 h culture by using an immunoprecipitation method, and the pFAK was quantified by Western blotting on specimens containing equal amounts of FAK. Figure 7 shows the results. The most significant result is that, for the same amount of FAK, the Fn-coated HC-patterned film exhibited 3 times higher pFAK expression compared with that of the flat film. The difference in focal adhesion pattern and the extent of FAK phosphorylation between HC-patterned and flat films clearly indicate that the signaling pathway of PAECs on an HC-patterned film differs from that on the flat films.

Focal adhesion formation and FAK phosphorylation are essential to a cell's ability to adhere. Integrin receptors recognize a specifically distinct peptide sequence of Fn (cell-binding RGD integrin recognition motif) that mediates cell-substrate focal

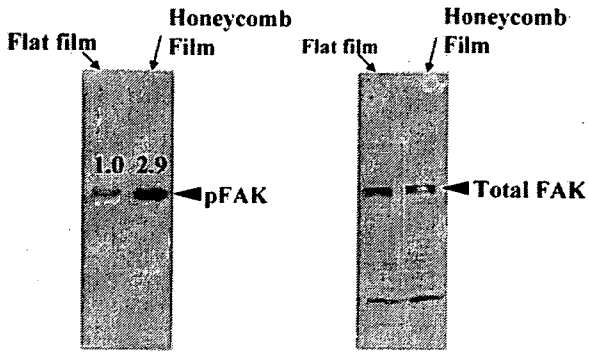

Figure 7. Representative Western blot of pFAK and FAK from PAECs plated on HC-patterned and flat films. Both films were precoated with Fn by 48 h incubation in a PBS solution of Fn. PAECs were then plated on the films and then cultured for 1 h. Values are the average relative amount of pFAK of three samples.

contact adhesion. The binding of adhesion receptors to adsorbed Fn provides mechanical coupling to the underlying substrate and activates signal-transductive pathways that control cellular behavior such as proliferation and differentiation.[40] Fn molecules were located in fibrillar form at the periphery of the micropores. In our current study, the adsorption sites of Fn corresponded well with the location of focal contact points, suggesting that the focal adhesion pattern on HC-patterned films is determined by the adsorption pattern of Fn. Focal contact points were regularly aligned on the HC-patterned films (Figure 5g–o). Such a regular adhesion pattern implies that the distance between adjacent focal contact points and/or the density of focal contact points is determined precisely by the pore size. Moreover, this distance and/or density might play a vital role in activating the signal-transductive reactions. The control of focal contact points by the pore might govern the PAEC response characteristics to an HC-patterned film.

(40) Buridge, K.; Charanowska-Wodnick, M. *Annu. Rev. Cell Dev. Biol.* **1996**, *12*, 463–518.

Conclusion

In this study, the role an HC-patterned film plays in the response of PAECs was demonstrated. The adsorption arrangement of Fn was determined by the micropatterned pore of the HC-patterned film. The focal adhesion of PAECs located on the periphery of the pores in such a film corresponded well with the adsorption sites of Fn, indicating that the focal adhesion pattern is controlled by the adsorption pattern of Fn, which, in turn, is determined by the pore structure of the film. Quantifying the extent of FAK phosphorylation revealed that the signal transduction mediated by the binding between Fn and integrin is activated more effectively on an HC-patterned film than on a flat film. The present study confirmed again our previous hypothesis that the adsorption and arrangement of the cell-adhesion protein, Fn, is determined by a substrate micropattern and affects the molecular binding sites of the proteins to its receptor in cells. This influence explains the difference in the PAEC response to an HC-patterned film compared with that to a flat film.

Acknowledgment. This study was supported by Special Coordination Funds for Promoting Science and Technology, Ministry of Education, Culture, Sports, Science and Technology, Japan (MEXT), and CREST-JST (Grants-in-Aid from the Japan Science and Technology Corporation). The authors would also like to acknowledge Dr. J. O. Eniwumide for his helpful comments.

LA7003326

Available online at www.sciencedirect.com
ScienceDirect
Biomaterials 28 (2007) 1752–1760
Biomaterials
www.elsevier.com/locate/biomaterials

Platelet adhesion to human umbilical vein endothelial cells cultured on anionic hydrogel scaffolds

Yong Mei Chen[a,d], Masaru Tanaka[b,d], Jian Ping Gong[a,e,*], Kazunori Yasuda[c,d], Sadaaki Yamamoto[d], Masatsugu Shimomura[b], Yoshihito Osada[a]

[a]*Graduate School of Science, Hokkaido University, Sapporo 060-0810, Japan*
[b]*Nanotechnology Research Center, Research Institute for Electronic Science, Hokkaido University, Sapporo 001-0021, Japan*
[c]*School of Medicine, Hokkaido University, Sapporo 060-0810, Japan*
[d]*Creative Research Initiative 'Sousei', Hokkaido University, Sapporo 001-0021, Japan*
[e]*SORST, JST, Sapporo 060-0810, Japan*

Received 17 August 2006; accepted 1 December 2006
Available online 22 December 2006

Abstract

In this work we describe experiments designed to understand the human platelet adhesion to human umbilical vein endothelial cells (HUVECs) cultured on various kinds of chemically cross-linked anionic hydrogels, which were synthesized by radical polymerization. HUVECs could proliferate to sub-confluent or confluent on poly(acrylic acid) (PAA), poly(2-acrylamido-2-methyl-propane sulfonic acid sodium salt) (PNaAMPS), and poly(sodium *p*-styrene sulfonate) (PNaSS) gels. The proliferation behavior was not sensitive to the cross-linker concentration of the gels. However, the platelet adhesion on the HUVECs cultured on these gels showed different behavior, as revealed by human platelet adhesion test in static conditions. Only a few platelets adhered on the HUVEC sheets cultured on PNaAMPS gels with 4 and 10 mol% cross-linker concentrations, and completely no platelet adhered on the HUVEC sheets cultured on PNaSS gels with 4 and 10 mol% cross-linker concentrations. On the other hand, a large number of platelets adhered on the HUVECs cultured on PAA gels with 1, 2 mol% cross-linker concentrations and PNaAMPS gel with 2 mol% cross-linker concentration. Furthermore, the study showed that promote of the glycocalyx of HUVECs with transforming growth factor-β_1 (TGF-β_1) decreased platelet adhesion, and degrade the glycocalyx with heparinase I increased platelet adhesion. The results suggested that the glycocalyx of cultured HUVECs modulates platelet compatibility, and the amount of glycocalyx secreted by HUVECs dependents on the chemical structure and cross-linker concentration of gel scaffolds. This result should be applied to make the hybrid artificial blood vessel composes of gels and endothelial cells with high platelet compatibility.

Keywords: Platelet adhesion; Hydrogel; Cell culture; Glycocalyx

1. Introduction

Blood compatibility is one of the basic required parameters of biomaterials, which is suitable for application as artificial blood vessel. It is well-known that the major problem of the artificial blood vessel is that blood clot occurs after a certain period of implantation, especially when the diameter of artificial blood vessel is smaller than 5 mm [1]. During the past decades, many studies have performed to understand the interaction of platelets with synthetic polymers, hoping to find materials that are compatible with the vascular system [2–9]. It has been shown that polymer surfaces modified by grafted polymers or anti-thrombogenic mediators reduce platelet adhesion [10–15]. However, blood compatibility of the modified polymers decreases with blood contacting time due to desquamation of the modified materials.

In the in vivo vascular systems, the inner surface of blood vessel is covered by a functional endothelial cell (EC)

*Corresponding author. Graduate School of Science, Hokkaido University, Sapporo 060-0810, Japan. Tel.: +81 11 706 2774; fax: +81 11 706 2774.
E-mail address: gong@sci.hokudai.ac.jp (J.P. Gong).

0142-9612/$ - see front matter © 2006 Elsevier Ltd. All rights reserved.
doi:10.1016/j.biomaterials.2006.12.005

monolayer which protects procoagulant activity. The EC surface is covered by a layer of glycocalyx of 0.5–3 μm in thickness [16], containing a large amount of proteoglycans (PGs). The main component of PGs is heparan sulfate PGs (HSPGs) (50–90%), which consist of core protein and heparan sulfate-type glycosaminoglycan [17,18]. It was reported that two kinds of HSPGs, prelecan and biglycan, exhibit antithrombin activity [19–21]. Prelecan actives antithrombin III by heparin-like sequences in the heparin sulfate chains, and biglycan actives heparin cofactor II by the dermatan sulfate chains. Perlecan-expressing cells completely prevent occlusive thrombosis, while injured arterial segments containing perlecan-deficient cells has a 23% thrombotic occlusion rate [22]. The study showed that transforming growth factor β_1 (TGF-β_1) can promote the synthesis of HSPGs when EC density is high [23]. On the other hand, heparinase can degrade HSPGs [24].

The ideal artificial blood vessel should have the structure similar to in vivo blood vessel and take full advantages of cell functions. Therefore, artificial blood vessel with EC monolayer on its inner wall has been expected to inhibit thrombosis. However, the blood compatibility of in vitro cultured ECs is poorly investigated [25]. It is doubtful that the in vitro cultured ECs have the same anti-thrombogenic function as that of ECs in vivo [26].

Hydrogels are expected as scaffolds for repairing and regenerating a wide variety of tissues and organs, due to their three-dimensional network structure and viscoelasticity, which are similar to the macromolecular-based extracellular matrix (ECM) in biological tissues [27,28]. We have found that bovine fetal aorta ECs (BFAECs) can spread, proliferate, and reach confluent on synthetic hydrogels with negative charges, such as poly(acrylic acid) (PAA), poly(2-acrylamido-2-methyl-propane sulfonic acid sodium salt) (PNaAMPS), and poly(sodium *p*-styrene sulfonate) (PNaSS), without surface modification with any cell adhesive proteins or peptides [29]. However, the platelet adhesion behavior of the ECs cultured on the gels is unclear.

In this work, we describe experiments designed to understand the human platelet adhesion to human umbilical vein ECs (HUVECs) cultured on various kinds of chemically cross-linked anionic hydrogels (Fig. 1). It was found that the platelet adhesion on the cultured HUVECs strongly dependents on the chemical structure and cross-linker concentration of hydrogels, and these results are associated with the amount of glycocalyx on the cultured HUVECs.

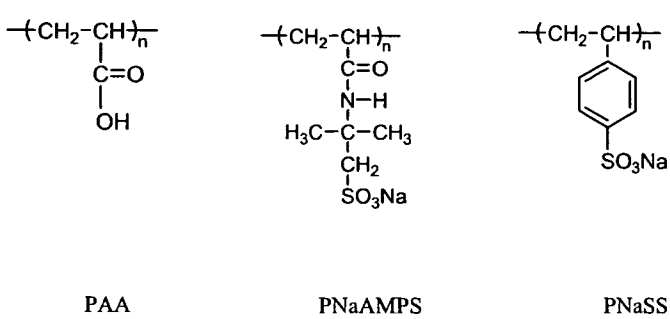

Fig. 1. Molecular structures of the polymers used in this work.

2. Materials and methods

2.1. Materials

2-Acrylamido-2-methyl-propane sulfonic acid sodium salt (NaAMPS) was obtained by neutralization of 2-acrylamido-2-methyl-propane sulfonic acid (Tokyo Kasei Kogyo, Tokyo, Japan) with sodium hydroxide in ethanol, and purified by recrystallization from acetone. Sodium *p*-styrene sulfonate (NaSS) and *N,N'*-methylenebis-(acrylamide) (MBAA) (Tokyo Kasei Kogyo, Tokyo, Japan) were purified by recrystallization from ethanol. Acrylic acid (AA) (Kanto Chemicals, Tokyo, Japan) was distilled at a reduced pressure. 2-Oxoglutaric acid (Wako Pure Chemicals, Osaka, Japan), sodium chloride, and sodium hydrogen carboxyl (Junsei chemicals, Tokyo, Japan) were used as purchased.

2.2. Hydrogel preparation

Hydrogels were synthesized and prepared as previously described [29]. Sheet-shaped gels were synthesized in the reaction cells that were formed by two parallel glass plates and separated by a silicone spacer of 1.5 mm thickness. An aqueous solution of 1 M monomer (AA, NaAMPS, or NaSS), 1–10 mol% cross-linker (MBAA), and 0.1 mol% initiator (2-oxoglutaric acid), was filled into the reaction cells. After being purged with nitrogen gas for 30 min, the cells were irradiated with UV light for polymerization (6 h).

After polymerization, gels were separated from the glass plates and immersed in a large amount of ion-exchanged water for 1 week. Water was changed two times every day to remove un-reacted residual chemicals. The gels were then immersed in 4-(2-hydroxyethyl) piperazine-1-ethanesulfonic acid sodium salt (HEPES) (Sigma, St. Louis, MO) buffer solution (HEPES 5×10^{-3} M, $NaHCO_3$ 1.55×10^{-2} M, NaCl 0.14 M, pH = 7.4). Phenol red (2.5×10^{-3} g/l) (Sigma, St. Louis, MO) was used to visualize the pH of the gels. After reaching equilibrium, the pH and ionic strength of solution containing in the gels was adjusted to 7.4 and c.a. 0.15 M, respectively. The thickness of equilibrated gels was about 2–3 mm. After sterilized by autoclaving (120 °C, 20 min), gel disks were punched out of the gel plates by a hole-punch with a radius of 1.5 cm. Then the gel disks were placed in a 24-well polystyrene (PS) tissue culture dish for HUVEC culture.

2.3. HUVEC culture

HUVECs (KURSBO Biomed. Bus., Tokyo, Japan) were cultured in Humedia-EB2 medium (KURSBO Biomed. Bus., Tokyo, Japan) containing 20% (v/v) fetal bovine serum (FBS) (GIBCO BRL Life Technologies, Inc., Gaithersburg, MD). 2.26×10^4 cells/cm^2 HUVEC suspension was seeded on the gel surfaces. The HUVECs-loading samples were cultured at 37 °C in a humidified atmosphere of 5% CO_2. The medium was changed every 24 h without damaging the HUVECs and the gels.

Floating HUVECs was counted with a haemocytometer at 6 h after seeding for determining the attached HUVEC number. The HUVEC morphology and proliferation on the gel surfaces were monitored using an Olympus IX 71 phase contrast microscope (Olympus, Japan) equipped with a digital camera using 10 × objective. The HUVEC monitoring was first performed at 6 h, and then monitored every 24 h, until the HUVECs proliferated to sub-confluent or confluent. HUVEC number counting was performed using the photography. More than four independent experiment runs were performed for each kind of gel. On each sample, four different areas were selected.

2.4. HSPGs modulation

TGF-β_1 (R&D Systems Inc., USA), which stimulates the HSPGs synthesis, was used to promote the amount of HSPGs on HUVEC surfaces [23,30]. Heparinase I (Sigma, St. Louis, MO), which cleaves heparin and heparin sulfate of HSPGs, was used to decrease the amount of HSPGs on HUVEC surfaces [31–33]. After proliferating to sub-confluent or confluent, HUVECs were incubated in 1 ml of 20 ng/ml TGF-β_1, which in serum containing medium, for 48 h, or 1 ml of 1.45 U/ml heparinase I, which in no serum containing medium, for 4 h.

2.5. Platelet adhesion test

Platelet adhesion test was performed in static conditions as previously described [3,4]. Human whole blood was drawn from healthy volunteer and mixed with a 1/9 volume of 3.8% sodium citrate. The blood was centrifuged at 1200 rpm for 5 min at room temperature for obtaining platelet-rich plasma (PRP). Then the residue was centrifuged at 3500 rpm for 10 min for obtaining platelet-poor plasma (PPP). The platelet concentration was determined by haemocytometer. The platelet density was adjusted to 1×10^5 cells/μl by mixing PRP and PPP. Then 200 μl (platelet number: 2×10^7) of the platelet suspension was loaded on the HUVECs proliferated to sub-confluent or confluent on PAA, PNaAMPS, and PNaSS gels, respectively, and incubated for 2 h at 37 °C. The bare poly(ethylene terephthalate) (PET) and PS plate, as well as the HUVECs proliferated to confluent on the PS plate were used as references. Hereafter, the HUVECs proliferated to confluent on the scaffolds is referred as HUVEC sheet.

After rinsing the weakly adhered platelets three times with phosphate buffer saline (PBS) (pH 7.4), adhered platelets were fixed by immersing the samples into 2.5 wt% glutaraldehyde of PBS for 2 h at 37 °C. Then the fixed samples were rinsed with PBS, 50% PBS, and ion-exchanged water. Samples were freeze-dried, and sputter-coated using a Pt–Pd target (E-1030, HITACHI) prior to observation by scanning electron microscope (SEM) (S-3500N, HITACHI). By counting the number of adhered platelets on the sample surfaces, the platelet adhesion densities were determined. More than three independent experimental runs were preformed for each kind of sample. On each sample, five different areas were selected.

2.6. Sample dehydration

For observing platelet morphology and counting the number of adhered platelets on cultured HUVECs by SEM, platelets, HUVECs, and the gels should be dehydrated without shape distortion. The conventional method to dehydrate the adhered platelets on the polymer modified solid scaffolds is not suitable for dehydrating the gel scaffolds with HUVECs and platelets [34]. Because in the process of conventional dehydration method, samples were treated by gradually exchanging solvent with ethanol/distilled water mixture (50–100% ethanol, 10% increment) before freeze drying. The process results in dramatic shrinkage of the gels, and most of the adhered platelets and HUVECs were exfoliated from the gel surfaces.

We solved this problem by the secondary freeze-drying operation (AdVantage Freeze Dryer Instruction, VIRTIS, Gardiner, USA). The process is as follow: after the temperature of freeze-drying chamber was decreased to −70 °C, the samples were put into the freeze-drying chamber and frozen at −70 °C for 2 h. The frozen samples were subsequently dehydrated at −40 °C for 5 h, −25 °C for 4 h, and 25 °C for 4 h. The vacuum was maintained at higher than 100 mTorr during the freeze-drying run. After the secondary freeze-drying, the size of the gels did not significantly changed, adhered platelets and HUVECs remained on the gel surfaces, keeping their original shapes.

3. Results and discussion

3.1. HUVECs growth on hydrogels

Cultivation of HUVECs on PAA, PNaAMPS, and PNaSS gels were performed. The gels were not modified with any cell adhesive proteins or peptides before HUVEC cultivation. The phase contrast micrographs of the HUVECs cultured on the PAA, PNaAMPS, and PNaSS gels, as well as on the reference, PS plate, at 144 h are shown in Fig. 2. The corresponding HUVEC densities on these scaffolds are shown in Fig. 3. HUVECs proliferate to confluent on the strong anionic gels, PNaAMPS (cross-linker conc. 2, 4, 10 mol%) and PNaSS (4, 10 mol%) at 144 h, with a cell density higher than 1.1×10^5 cell/cm^2, closed to that on PS plate. On the other hand, HUVECs proliferated to sub-confluent on the weak anionic PAA (1, 2 mol%) gel with a cell density of about 4.5×10^4 cell/cm^2.

Fig. 4 shows the HUVECs densities on PAA (1, 2 mol%), PNaAMPS (4 mol%), and PNaSS (10 mol%) gels, as well as on PS plate, as a function of culture time. HUVEC proliferation rates on 2 and 10 mol% PNaAMPS gels were the same as that on the 4 mol% PNaAMPS gel, and the cell proliferation rate on the 4 mol% PNaSS gel was the same as that on the 10 mol% PNaSS gel (data are not shown). It shows that the HUVEC proliferation rate on various scaffolds increases in the order of PAA $<$ PNaAMPS $\approx$ PNaSS $\approx$ PS. In addition, the HUVEC proliferation rate is not dependent on the cross-linker concentration of the gels. The results are in agreement with our previous study on BFAECs cultured on PAA, PNaAMPS, and PNaSS gels, indicating that the ECs proliferation rate correlates with the charge density of negative charged gels [29].

3.2. Platelet adhesion on the HUVECs cultured on hydrogels

PET plate that is often used as a negative control scaffold of platelet adhesion [35,36], and PS plate that is often used as a cultivation scaffold of anchorage-dependent cells [37], were chosen as references for platelet adhesion test. The morphology of the adhered platelets (spherical shape, spreading shape, and pseudopodia extension) observed by SEM images is one of the indexes expressing the degree of the platelet activation [3–5]. SEM images of the adhered platelets on the HUVEC sheets cultured on various gels, and on the references, i.e. bare PET, PS, and the HUVEC sheet cultured on the PS, are shown in Fig. 5, the corresponding densities of adhered platelets on these samples are shown in Fig. 6.

Figs. 5 and 6 show that a large amount of platelets adhere on the bare PET plate (271 cells/10^4 μm^2), and 53.9% of all adhered platelets are spreading, 43.1% platelets are rounded with pseudopodia extension, indicating the activation of the platelets. Except on the bare PET plate, the platelets that adhere on the cultured HUVECs

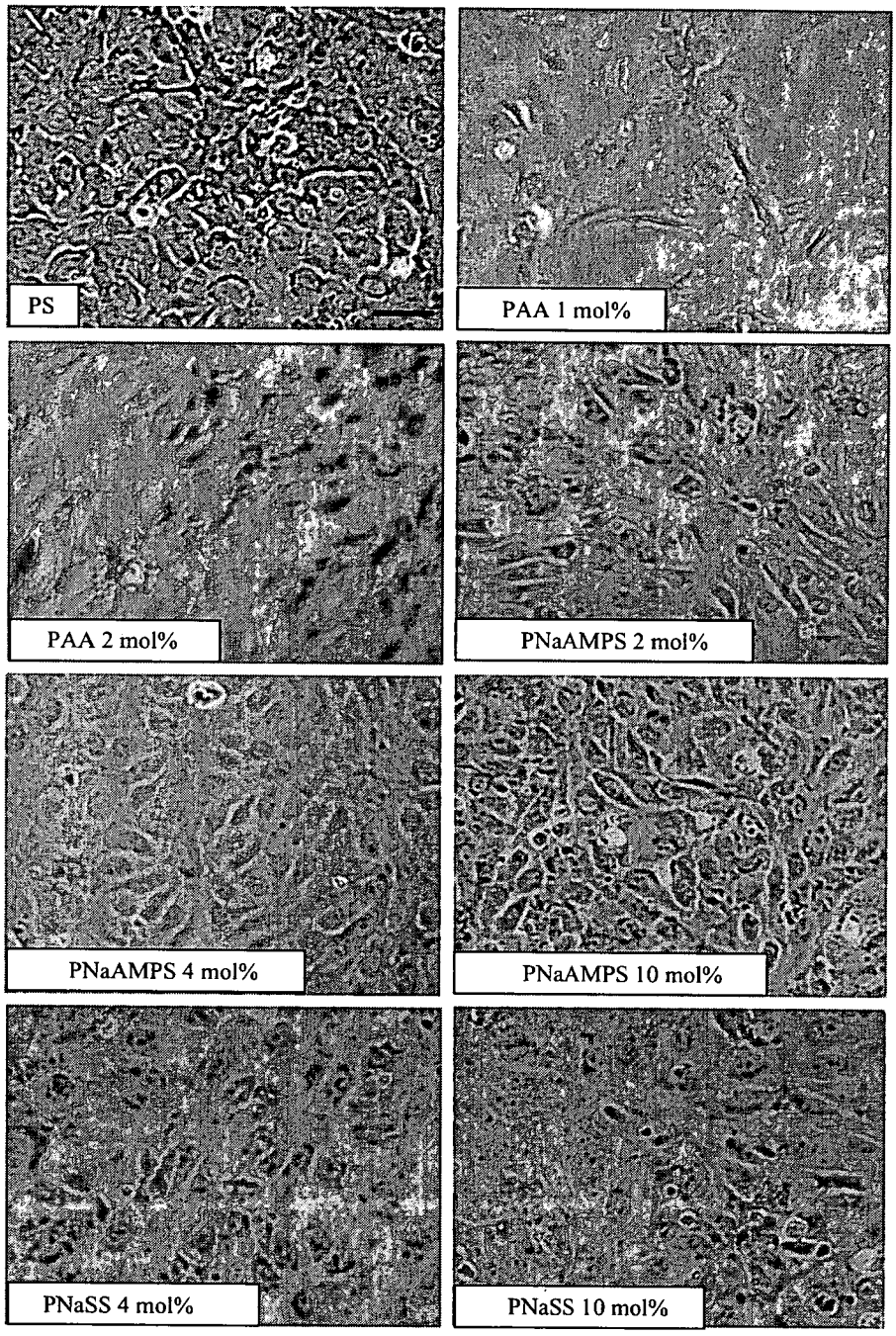

Fig. 2. Phase-contrast micrographs of the HUVECs cultured on various kinds of substrates at 144 h. The numbers in the figures are the concentration of MBAA in molar ratio in relative to monomer used in gelation. Scale bar: 100 μm.

and on the bare PS plate keep their original spherical shape, indicating not activate of the platelets. The density of adhered platelets on the HUVEC sheet cultured on the PS plate (185 cells/10^4 μm^2) is obviously lower than that on the bare PS plate (320 cells/10^4 μm^2). It shows that the HUVEC sheet cultured on the PS plate inhibits platelet adhesion comparing with the bare PS plate.

The platelets showed a similar adhesion behavior on the HUVECs cultured on the weak anionic PAA gels, and platelet adhesion on the HUVECs cultured on the PAA gels is not dependents on the cross-linker concentration of the gel. The density of adhered platelets on the as-prepared HUVECs cultured on PAA gels is 115 cells/10^4 μm^2. It should be noted that the HUVECs proliferate to sub-confluent on PAA gels, therefore, when the platelet suspension was cast on the HUVECs cultured on PAA gel, platelets could adhere on both of the HUVECs surface and on the PAA gel surface where no HUVECs exist. We can clearly distinguish the adhered platelets on the HUVECs surface from the adhered platelets on the PAA gel surface where no HUVECs exist by SEM images (Fig. 5).

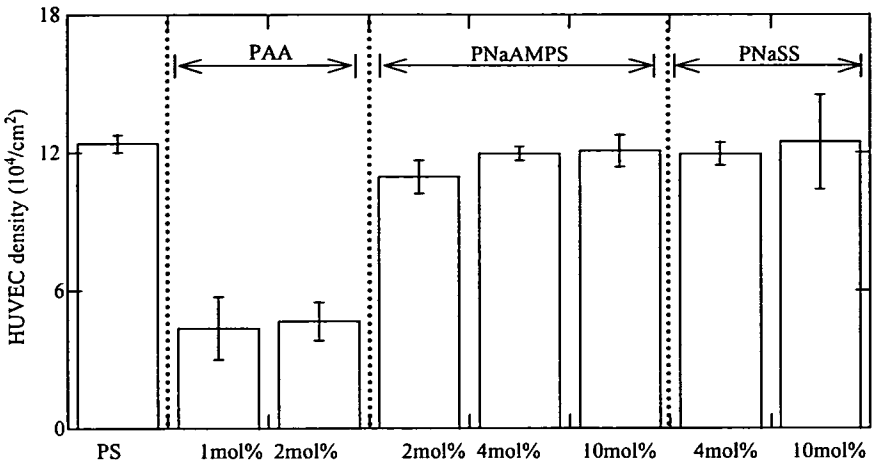

Fig. 3. Densities of the HUVECs that proliferate to confluent or sub-confluent on various kinds of scaffolds at 144 h. The numbers in the figures are the concentration of MBAA in molar ratio in relative to monomer used in gelation. Error ranges are standard deviations over $n = 4$–6 samples.

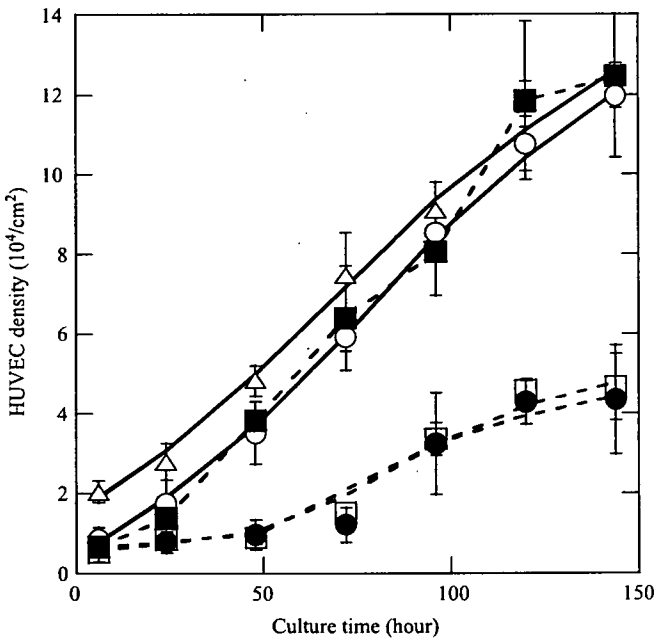

Fig. 4. Densities of the HUVECs cultured on various kinds of scaffolds as a function of culture time. (○) PNaAMPS (4 mol%), (■) PNaSS (10 mol%), (●) PAA (1 mol%), (□) PAA (2 mol%), (△) PS plate. Error ranges are standard deviations over $n = 4$–8 samples.

When the cross-linker concentration of PNaAMPS gel is 2, 4, and 10 mol%, the density of adhered platelets on the as-prepared HUVEC sheets is 183, 34, and 6 cells/10^4 μm^2, respectively. It shows that the platelet adhesion on the HUVEC sheets cultured on the strong anionic PNaAMPS gels decreases with increasing the cross-linker concentration of the gel.

It is a surprising result that no platelets adhere on the HUVEC sheets cultured on the PNaSS gels, regardless the cross-linker concentration (4 and 10 mol%) of the gel.

The above results demonstrated that the anti-platelet adhesion of the HUVECs cultured on various scaffolds increases in the order of PS < PAA < PNaAMPS < PNaSS, indicating that the platelet compatibility of the HUVECs cultured on these anionic gels is higher than that of PS plate. In addition, the ability of platelet adhesion on HUVECs depends on the chemical structure and cross-linker concentration of the gels used as scaffolds for HUVEC cultivation.

It was reported that EC glycocalyx relates to platelet adhesion [22,40]. We hypothesize that the glycocalyx, synthesized by HUVECs, is affected by the chemical and physical properties of the gels. To verify this, we modulated the glycocalyx on the cultured HUVECs, and studied its influence on the platelet compatibility.

The amount of glycocalyx is increased by a kind of cytokine, TGF-β_1, which promotes ECs to synthesize HSPGs, the main component of the PGs. It was demonstrated that TGF-β_1 treatment is able to increase more than 50% of HSPGs on EC surface. Furthermore, the glycolsaminoglycan chains of bioglycan synthesized by the ECs were elongated [23]. On the other hand, the amount of glycocalyx is decreased by a kind of enzyme, heparinase I, by cleaving glycolsaminoglycan side-chains from HSPGs [31–33]. It was demonstrated that heparinase treatments were able to reduce 27–51% fluorescence intensity of fluorescence-labeled wheat germ agglutinin [38], and reduce 45.9% of fluorescence intensity associated with heparin sulfate antibody [32].

Here, we use TGF-β_1 and heparinase I to treat the as-grown HUVECs and their adhesion to platelets were investigated. The SEM images of the adhered platelets on TGF-β_1 or heparinase I treated HUVECs cultured on various kinds of gels is shown in Fig. 7, the corresponding densities of adhered platelets on these samples are shown in Fig. 6. The morphology of adhered platelets on heparinase I treated HUVECs cultured on 1 mol% PAA gel was the same as that on 2 mol% PAA gel, and the morphology of adhered platelets on TGF-β_1 treated HUVECs cultured on 4 mol% PNaAMPS gel was the same as that on 2 mol% PNaAMPS gel (data are not shown).